Improving river networks hydrological-hydraulic models with SWOT and multi-satellite data

Kévin Larnier, Pierre-André Garambois, Charlotte Emery, Léo Pujol, Jérôme Monnier, Laetitia Gal, Adrien Paris, Hervé Yesou, Thomas Ledauphin, Stéphane Calmant

Improving river networks hydrological-hydraulic models with SWOT and multi-satellite data

Kévin Larnier[1], Pierre-André Garambois[2], Charlotte Emery[3], Léo Pujol[2], Jérôme Monnier[4], Laetitia Gal[1], Adrien Paris[1], Hervé Yesou[6], Thomas Ledauphin[6], Stéphane Calmant[1]

[1]Hydro Matters, Toulouse, France

[2]INRAE, Aix-Marseille Université, RECOVER, Aix-en-Provence, France

[3]CS Group, Toulouse, France

[4]INSA, IMT, Toulouse, France

[5]CPRM, Brazil

[6]SERTIT, ICube, Strasbourg University, France

Key Points:

- Improvement of a differentiable 1D Saint-Venant river network model with variational data assimilation of SWOT data at basin scale.
- Simultaneous and physically consistent estimation of large spatio-temporal inflows, bathymetry and friction of hydraulic network model.
- Automatic pre-processing of multi-satellite altimetry and images for basin scale model setup and wavelet-based filtering of SWOT L2 RiverSP data at node scale.

Abstract

The unprecedented hydraulic visibility of rivers surfaces deformation with SWOT satellite is tremendous information for refined hydrological-hydraulic modeling. But the estimation of uncertain or unknown discharge and bathymetry-friction in a spatialized hydrodynamic model from water surface elevation (WSE) and width (WSW) observations is a difficult high-dimensional inverse problem faced with equifinality. This article newly studies variational data assimilation (VDA) of WSE into a 1D Saint-Venant differentiable river network model fed by a semi-distributed hydrological model. A pre-processing chain enables (i) building effective hydraulic model geometry from WSE altimetry (Sentinel 3, drifting ICESat2) and WSW (Sentinel 1 images), and (ii) filtering noisy SWOT level 2 WSE before assimilation. The simultaneous inference of spatially distributed inflow hydrographs, bathymetry-friction at network scale, on the large poorly gauged Maroni basin (French Guiana), is done by VDA of nadir and in situ WSE or SWOT 1-day WSE only. A systematic improvement obtained for the fit to assimilated WSE and in validation of discharge at 5 gauges inside the network: 70% of data-model misfit in $[-0.25\ ;\ 0.25m]$, NRMSE on discharge between 0.11 and 0.26 for SWOT only on a large flood given unfavourable hydrological prior. SWOT

Corresponding author: Pierre-André Garambois, pierre-andre.garambois@inrae.fr

WSE density enables to infer detailed spatial variability on channel bottom elevation given width from images and detailed temporal variabilities of hydrological inflow hydrographs. The approach is transposable to other rivers networks worldwide in view to tackle the double regionalization problem of hydrological and hydraulic parameters from sparser but increasingly massive and informative data.

Keywords: Satellite data of SWOT, ICESat2 and Sentinel 3 altimetry, Sentinel 1 images, for hydraulic modeling; Differentiable 1D Saint-Venant river network model, numerical adjoint model and variational data assimilation algorithm; Simultaneous inference of spatially distributed river network bathymetry, friction and inflows; High-dimension optimization and improved fit to altimetry water heigths and discharge in validation; Poorly gauged bassins

1 Introduction

Improving the estimation of freshwater stocks and fluxes in surface hydrology is an important scientific question that is essential to address regarding major socio-economic issues such as water resource management or forecasting of extremes (floods and droughts), especially in the context of climate change and potential intensification of the water cycle (Masson-Delmotte et al., 2022). Elaborating detailed and reliable hydrological-hydraulic models, capable to translate atmospheric signals into river flows and inundations depths, velocities and extents, while integrating the available observations of these flows, for scientific research and decision support, is crucially needed. However, the more complex the desired or required modelling, the more information is required to constrain it.

Hydrological-hydraulic modeling generally requires data to describe (1) atmospheric forcings, (2) physical properties of the catchment (drainage, topography, land use, composition of the soil and subsoil, etc) and the hydrographic network (bathymetry, hydraulic friction, structures), as well as flow observations (discharge and water depth at the very least, flow velocities, slopes, soil moisture, etc) to estimate the model parameters. Discharge data, which are crucial to calibrate rainfall-runoff hydrological models, are more or less rare depending on the basins and the spatial density of their ground measurement networks, they integrate the signature of the complex combination of physical processes occurring in the compartments of the upstream basin (rivers, lakes, biosphere, aquifers and unsaturated soils, cf. Milly (1994)) with significant spatio-temporal variabilities (e.g. Flipo et al. (2014); Schuite et al. (2019)), and such discharge data contain uncertainty (e.g. Mansanarez et al. (2016); Horner et al. (2018); Eggleston et al. (2024)). Bathymetry and friction data are needed to constrain hydraulic modeling and are unvailable in many areas. Dry bahtymetry can be measured accurately with airborne LiDAR while wet bathymetry, i.e. below river surface, requires in situ surveys or penetrating LiDAR in clear shallow streams (cf. Lague & Feldmann (2020)). The friction of hydraulic models can only be estimated indirectly from flow measurements. In complement to in situ data, new generations of earth observation satellites and sensors provide increasingly accurate an spatially dense measurements of water surface variabilities of worldwide rivers, especially on remote and hardly measurable ones, in terms of water surface elevation Z, width W and slope S.

This hydraulic visibility yielded by single or multi-satellite measurements, i.e. *the potential to depict a hydrological response and surface hydraulic variabilities within a river section or network via remote sensing* (Garambois et al. (2017), see also Rodríguez et al. (2020)) can provide valuable information for estimating discharge with a local discharge law function of flow geometric parameters (rating curves in Z and Z, S (Paris et al., 2016) or in W (Pavelsky, 2014) or stage-fall-discharges or Low Froude model in Z, S (Malou et al., 2021)) depending on the uncertainties on bathymetry and friction which are key hydraulic parameters that are unobservable from space (cf. Larnier et al. (2020); Frasson et al. (2021)), or even for calibration of reach scale or network scale hydraulic models (e.g. Paiva et al. (2013); Garambois et al. (2017); Schneider et al. (2017); Garambois et al. (2020); Pujol et al. (2020); Malou et al. (2021); Coppo Frias et al. (2022)). Nevertheless, the estimation of hydraulic model parameters from water surface (WS) observables can result in more or less difficult and ill-posed inverse problems depending on the complexity of the physical system and of the model used, on the nature and amount of observations and unknowns.

Discharge Q of gradually varied flows (cf. Chow (1959); S. Dingman (2009)) can be related, locally at a section or river reach scale, to flow energy slope S_f such that:

$$Q = \kappa S_f^{1/2} = \prod_{i=1}^{N} p_i^{\alpha_i} \tag{1}$$

with κ the flow debitance which is inversely proportional to a friction parameter ρ such that $p_1 = 1/\rho$ and proportional to the product of the flow parameters p_i raised to the corresponding exponent α_i (cf. S. Dingman (2009); Rodríguez et al. (2020)). Theoretically, an infinity of friction parametrizations is possible, those of Chézy, Manning-Strickler or Darcy–Weisbach being commonly used in free surface hydraulics (cf. Chow (1959); S. Dingman (2009), e.g. Kirstetter et al. (2016)). Note also the link with the power laws of hydraulic geometries and with geomorphological variability (Leopold & Maddock, 1953), see application to recent datasets and analysis in S. L. Dingman & Afshari (2018); Eggleston et al. (2024) and references therein). Given the relatively large scales of satellite measurements, the flows observed can be considered stationnary and mainly Low Froude, i.e. Fr ≤ 0.3, the friction slope S_f equals the surface slope $S = |\partial_x Z| > 0$, and the low Froude Manning Strickler model writes (cf. Garambois & Monnier (2015)):

$$Q = KAR_h^{2/3}\sqrt{S} \tag{2}$$

Where K is the Strickler friction coefficient, A and R_h are respectivey the wetted flow section and hydraulic radius depending on bathymetry b and cross-section (XS) geometrical shape. Discharge estimation from WS observations only, with unknown bathymetry b and friction K embedded in the low Froude Manning-Strickler model, is an ill-posed inverse problem (cf. Garambois & Monnier (2015); Larnier et al. (2020)) and an accurate mean or a reference value of one of the sought parameters (Q, K, b) is required to perform accurate estimates (Larnier et al., 2020; Larnier & Monnier, 2023). When reliable discharge data, either given by ground-based measurements or by a river network model, are available for calibration of flow laws, stage-discharge (rating curve, $Q = aZ^b$) or stage-fall-discharge laws ($Q = cZ^dS^e$, e.g. Paris et al. (2016); Malou et al. (2021)) or the low Froude Manning Strickler model, can provide accurate discharge estimates. The accuracy of satellite-based discharge estimate depends on observation errors, flow law parameters error and structural model errors Yoon et al. (2016); Larnier et al. (2020); Durand et al. (2023). Site-specific geomorphic and hydraulic conditions affect both ground-based (e.g. Le Coz et al. (2014); Mansanarez et al. (2016)) and satellite-based river flow monitoring (Frasson et al., 2021; Eggleston et al., 2024).

The satellite-based hydraulic visibility of river flow signatures through water surfaces deformations can be used to calibrate parameters of reach scale or river network scale hydrological-hydraulic models. For example, the MGB model (Portugese acronym - Modelo de Grandes Bacias, (Collischon et al., 2007; Pontes et al., 2017)) with simplified non inertial 1D hydraulics, yet of sufficient realism to enable ingesting water surface elevation (WSE) data, has been calibrated with ENVISAT altimetric data in Getirana (2010); Paiva et al. (2013) and with multi-satellite data in Meyer Oliveira et al. (2021), it has been corrected with assimilation of synthetic SWOT WSE, WSE and discharge with a Kalman filter at basin scale in Wongchuig-Correa et al. (2020). The friction of a simplified 1D hydraulic model of an anastomosed reach, with equivalent 1D XS geometry with low and high flow width from satellite images (JERS2) and effective bottom elevation from altimetric rating curves of Paris et al. (2016), fed by discharge of the MGB model, has been calibrated with ENVISAT altimetry in Garambois et al. (2017). Triangular XSs of a 1D dynamic wave model, fed by discharges of a pre-calibrated semi lumped hydrological model, have been calibrated (bottom elevation and shape parameter) with CryoSat-2 drifting altimetry data in Schneider et al. (2017). A low-parameterized steady hydraulic model, i.e. with spatially uniform 2 parameters XS shape and friction, has been calibrated with a global search algorithm using ICESat-2 altimetry data in Coppo Frias et al. (2022).
These studies investigated low-dimensional calibration problems with classical global search algorithms. More advanced estimation algorithms are required for the estimation of high-dimensional spatially distributed parameters of river network hydrodynamic models, in view to best approximate the available flow observations while reducing modeling errors which are both spatio-temporally varied.

The Variational Data Assimilation (VDA) approach (cf. Cacuci et al. (2013) and references therein, also Monnier (2021)) is well suited to estimate large parameters vectors of full hydraulic models (see Brisset et al. (2018); Oubanas et al. (2018); Larnier et al. (2020) with synthetic SWOT data Tuozzolo et al. (2019); Garambois et al. (2020); Pujol et al. (2020); Malou et al. (2021) with real data). This method aims to minimize the fit, in the sense of a given cost function, between the model response and observed data, by optimizing model parameters. Optimization algorithms adapted to high-dimensional inverse problems, such as the LBFGS or Adam algorithms, require the computation of the cost gradient to the sought parameters, which can be computed from the numerical adjoint model of a differentiable numerical forward model (cf. Monnier (2021)). The simultaneous estimation, from WS observables, of spatio-temporal hydraulic parameters, i.e. inflow discharge $Q(t)$ and bathymetry $b(x)$ and friction $K(x)$ is a difficult inverse problem given their correlated influence on simulated WS and regularizations are needed for solving it (cf. Larnier et al. (2020); Garambois et al. (2020) and references therein). As before for local discharge laws, parameters inversion from WS observables is faced with model structural equifinality (sought parameters being embedded into the friction source term) but also to spatial equifinality, i.e. spatial patterns of parameters leading to similar model fit to observations (see analysis for hydraulic modeling from WS observations in Garambois et al. (2020) in 1D, Pujol et al. (2024) in 2D). The spatial density of WSE measurements brought by SWOT, and the visibility of flow lines offer new possibilities to estimate spatially distributed parameters. However, satellite altimetry measurements of WS are relatively sparse in time compared to local flow dynamics. This important aspect of the inverse problem is investigated in Brisset et al. (2018) with the introduction of the identifiability maps which represent in space-time the available information: WS observables, hydraulic waves and an estimation of the misfit with the local hydraulic equilibrium. These maps enable to estimate if the sought upstream discharge information has been observed or not within the downstream river surface deformations; also they help to estimate inferable hydrograph frequencies Brisset et al. (2018) or inferable hydrograph time windows Larnier et al. (2020) at reach scale, and have been applied on a long reach of the Negro River with several tributaries and synthetic SWOT data Pujol et al. (2020). The variational assimilation of multi-satellite observations into a river network scale differentiable hydraulic model has seldom been done and would enable maximizing information extraction for estimating large vectors of spatio-temporal model parameters.

This article newly studies the improvement of integrated hydrological-hydraulic (H&H) models, of a river network within its basin, that can be obtained by leveraging the unprecedented hydraulic visibility from the recently launched SWOT satellite in complement of altimetry and imagery from other state-of-the-art satellites used to build the prior model geometry. It presents the first application of VDA over a differentiable river network 1D Saint-Venant hydraulic model fed by a semi-distributed hydrological model over a poorly gauged basin. Moreover, the approach builds on a proposed automatic pre-processing chain enabling to build a hydraulic model geometry from multi-satellite data, on a hydraulic preserving wavelet-based filtering algorithm for SWOT L2 RiverSP products at node scale, on a differentiable hydrodynamic solver and VDA algorithm, with the following original ingredients all applicable to open source data and other basins worldwide:

- A pre-processing algorithm for water surface width (WSW) extraction from optical and radar images, for WSE extraction from ICESat2 altimetry, both used to build the a priori river geometry.
- A fine analysis and filtering of 1D L2 SWOT river products, with a wavelet-based processing algorithm based on Montazem et al. (2019) with some upgrades.
- A network scale differentiable 1D Saint-Venant hydraulic model, DassFlow1D, fed with discharge from the pre-calibrated MGB hydrological model for (i) a coherent state-flow modeling over river network at basin scale, (ii) while enabling sufficiently complex hydraulic modeling to fit high resolution observations of rivers surface deformations.

- A variational data assimilation (VDA) algorihtm enabling to ingest multi-source heterogenous data and to estimate high-dimensional spatio-temporal model parameters, here spatially distributed bathymetry, friction and inflow hydrographs of the hydraulic model.

The remainder of this article is as follows: section 2 presents the modeling approach and the inverse algorithm, section 3 presents the studied case and data, results and discussions are detailed in section 4, conclusion and perspectives are given in section 5.

2 Flow model and data assimilation algorithm formulation

This section successively presents (1) the forward river network model composed of the differentiable 1D Saint-Venant hydraulic network model, DassFlow1D, fed with discharges from the semi-distributed hydrological model MGB; (2) the variational data assimilation algorithm (Figure 1); (3) the studied Maroni River basin (MRB) and multi-source data (Figure 2), and the automatic chain for data processing (Figure 3 and 4), model meshing and coupling (Figure 5), (4) the modeling and data assimilation hypothesis and the numerical experiment design.

2.1 Forward river network flow model

2.1.1 Hydrological-hydraulic coupling

We consider a 2D river basin domain Ω_{rr}, on which is applied a spatialized hydrologic model $\mathcal{M}_{rr}$, that contains a sub-domain Ω_{hy} on which is applied a 1D $\mathcal{M}_{hy}$ hydraulic model of the river network. This hydraulic model is fed by the hydrologic model through discharge time series at N_{in} inflow points, with N_{up} upstream and N_{lat} lateral inflow points, determined by preprocessing as explained later. This coupling interface between the hydrological and hydraulic model is denoted $\Gamma_{in} = \Gamma_{up} \bigcup \Gamma_{lat}$ and is the coupling interface with the hydrological model that provides mass flux time series, i.e. inflow hydrographs to the hydraulic model at upstream and lateral inflow points.

The meshing of the hydrological domain Ω_{rr} consists here in a drainage plan composed of topographical sub basins. The hydraulic domain Ω_{hy}, $\Omega_{hy} \subset \Omega_{rr} \subset \mathbb{R}^2$, is a portion of a hydrographic network plus its floodplains, described by connected segments $s = 1..N_{seg}$ defined between upstream inflow points and successive confluences; $t \in]0, T]$ denotes the physical time and $x \in \Omega_{hy}$ the curvilinear abscissa within a segment s.

The obtained hydrological-hydraulic model, weakly coupled via hydrological fluxes imposed at upstream boundary conditions and lateral mass source terms, is denoted as:

$$\mathcal{M} = \mathcal{M}_{hy}\left[K(s,x), b(s,x), Z_{down}(t), \left(Q_{in,1..N_{BC}}, Q_{lat,1..N_{lat}}\right)(t) = \mathcal{M}_{rr}\left(.\right)\right] \tag{3}$$

Where $K(s,x)$ and $b(s,x)$ respectively denote the spatially distributed hydraulic friction coefficient and bathymetry, $Z_{down}(t)$ is the water level time series used as downstream boundary condition (BC), and $Q_{in,1..N_{up}}(t)$ (resp. $Q_{lat,1..N_{lat}}(t)$) the $N_{in} = N_{up} + N_{lat}$ inflow hydrographs used as upstream BC (resp. lateral source term) of the hydraulic model written after.

2.1.2 1D Saint-Venant hydraulic model

The hydraulic model is written here for a given segment s composing the river network domain Ω_{hy}. Let $A(x,t)$ $[\mathrm{m}^2]$ be the XSal area of flow and $Q(x,t)$ $[\mathrm{m}^3/\mathrm{s}]$ the flow rate such that $Q = UA$ with $U(x,t)$ the mean velocity [m/s] over a XSal area of flow. The Froude number for any XS is defined as $\mathrm{Fr} = {}^{U}/_{c} = \sqrt{{}^{Q^2W}/_{gA^3}}$, where W is the top width, and compares the flow velocity U with the wave velocity c; Fr^2 compares the kinetic energy of the moving fluid with the potential energy of gravity.

The 1D Saint-Venant equations taking into account a variable XS A with lateral fluxes of exchange q_l, write as follows:

$$\mathcal{M}_{hy}: \quad \partial_t \mathbf{U} + \partial_x \mathbf{F}(\mathbf{U}) \ = \ \mathbf{S}(\mathbf{U})$$

$$\mathbf{U} = \begin{bmatrix} A \\ Q \end{bmatrix}, \ \mathbf{F}(\mathbf{U}) = \begin{bmatrix} Q \\ \beta \frac{Q^2}{A} \end{bmatrix}, \ \mathbf{S}(\mathbf{U}) = \begin{bmatrix} q_l \\ -gA\left(\frac{\partial Z}{\partial x} - S_f\right) + U\delta_l q_{lat} \end{bmatrix} \tag{4}$$

where $Z(x,t)$ is the WSE $[m]$ and $Z = (z_b + h)$ with $z_b(x)$ the river bed level $[m]$ and $h(x,t)$ the water depth $[m]$, $R_h(x,t) = A/P_h$ the hydraulic radius $[m]$, $P_h(x,t)$ the wetted perimeter $[m]$, g is the gravity magnitude $\left[m.s^{-2}\right]$, $q_{lat}(x,t)$ is the lineic lateral discharge $\left[m^2.s^{-1}\right]$ and δ_l is a lateral discharge coefficient chosen equal to one here since we consider inflows only. Let us recall the Froude number definition $\mathrm{Fr} = U/c$ comparing the average flow velocity U to pressure wave celerity $c = \sqrt{\frac{gA}{W}}$ where W is the flow top width $[m]$. β is a dimensionless coefficient accounting for velocity non-uniformity and set to 1 by default.

2.1.3 Friction parameterization

The friction term S_f is classically parameterized with the empirical Manning-Strickler law established for uniform flows

$$S_f = \frac{|Q|Q}{K^2A^2R_h^{4/3}} \tag{5}$$

where $K(x)$ $\left[\mathrm{m}^{1/3}.\mathrm{s}^{-1}\right]$ is the Strickler coefficient that can be spatially distributed. A richer formulation is used here:

$$K(x,h) = \alpha(x)h^{\beta}(x) \tag{6}$$

More complex friction parameterization, such as the classical two-bed formulation Nicollet & Uan (1979) is available in DassFlow1D, and will be investigated in further research in case where more complex modeling is relevant (regarding flow complexity, bathymetry and flow data availibility).

2.1.4 Observation dataset and XS geometry parameterization.

The XS geometry can be defined classically from river channel and floodplain bathymetric data if available or from satellite observations of rivers surfaces for ungauged reaches. In this last case, with WS observations only, a part of the bathymetry remains unobservable below the lowest WS elevation measurement and an equivalent representation is generally used (cf. Durand et al. (2014); Garambois et al. (2017); Larnier et al. (2020) with SWOT-like data).

We denote by $\boldsymbol{Y}^*$ the set of multi-source observations of hydraulic responses over the river network domain Ω_{hy} that we aim to integrate into the flow model. This set consists in altimetric WSE and flow top width, unevenly spaced but rather densely covering the whole spatial domain (imagery, drifting or wide swath altimetry in addition to multi-mission nadir altimetry).

In the general case, a multi-satellite dataset, composed of WS elevation and width observations can be written as:

$$\boldsymbol{Y}^* := \left\{ (Z^*((s,x)_{vs=1..N_z}, t_{pz=1..P_z(oz)}); W^*((s,x)_{ws=1..N_w}, t_{pw=1..P_w(ow)}) \right\} \tag{7}$$

with $(s,x)_\square$ denoting the spatial location of WSE or WSW measurements sorted in ascending order of magnitude with $t_\square$ the observation times at this location; N_z (resp. N_w) being the number of WSE (resp. WSW) observation points accross the river network domain Ω_{hy}, and N_{oz} (resp. N_{ow}) the number of observation times for each WSE measurement location $x_{oz=1..N_z}$ (resp. WSW location $x_{ow=1..N_w}$). Similarly, $t_\square$ denotes measurements times.

In the case of SWOT, Z and W measurements are synchronous in time and space, and the dataset reduces to:

$$\boldsymbol{Y}^* := (Z^*, W^*)(x_{o=1..N_o}, t_{p=1..p(o)}) \tag{8}$$

In this work, SWOT width is not used but dynamic water masks are extracted from Sentinel radar data as explained after. This enables to define XSs geometries consisting in a rectangle for the unobserved lower part of the main channel, plus a superimposition of trapeziums above (cf. Larnier et al. (2020)). Over the studied basin are simple rectangular XS shape is used, which is justifiable by the low variability found in dynamic water masks a reasonable hypothesis (same hypothesis in the "neighbouring" Rio Negro basin on the other side of the Guiana shield in Pujol et al. (2020); Malou et al. (2021)) as shown by results accuracy after.

More complex parameterisation of XS shape, as the power law hydraulic geometry of S. L. Dingman & Afshari (2018) (e.g. used at reach scale in a SWOT discharge algorithm in Andreadis et al. (2020)) and a superimposition of dissymmetric trapeziums constrained from dynamic water masks (e.g. Brisset et al. (2018); Larnier et al. (2020)) available in DassFlow1D, could be investigated in further research in case more complex modeling is pertinent (again regarding flow complexity and data availibility).

2.1.5 Hydrological-hydraulic model and numerical resolution

First, consider a distributed or semi-distributed hydrological model $\mathcal{M}_{rr}$ providing spatio-temporal discharges estimates $Q_{rr}(x',t)$, $\forall x' \in \Omega_{rr}, \forall t \in [0,T]$ that are used to inflow the hydraulic model at N_{in} inflow points, either upstream boundary conditions and lateral inflows, at the border of the hydraulic domain Ω_{hy}.

The 1D Saint-Venant equations are solved on each segment of the river network and the continuity of the flow between segments is ensured by applying an equality constrain on water levels and mass conservation at the confluence between two segments.

Boundary conditions (BCs) are classically imposed (subcritical flows here) at boundary nodes (main hydrological inflows here) with inflow discharges $Q_{in,i=1..N_{BC}}(t)$ at N_{BC} upstream nodes and WSE $Z_{avl}(t)$ at the downstream node; lateral hydrographs $q_{lat,i=1..N_{lat}}(t)$ at N_{lat} lateral inflow nodes (such that $N_{in} = N_{BC} + N_{lat}$). The initial condition is set as the steady state backwater curve profile $Z_0(x) = Z(Q_{in}(t_0), q_{lat,1..L}(t_0))$ for hot-start. This 1D Saint-Venant model is discretized using the classical implicit Preissmann scheme (see e.g. Cunge et al. (1980); Roux (2004)) on a regular grid of spacing Δx using a double sweep method enabling to deal with flow regimes changes; hourly time step Δt here. This is implemented into the computational software DassFlow1D. See DassFlow documentation (https://dasshydro.github.io/doc/); accurate finite volume scheme are also available; source code on GitHub (https://github.com/DassHydro/dassflow1d).

2.2 Variational data assimilation algorithm

The estimation of spatially and temporally distributed controls (bathymetry, friction, inflow discharges) of the river network hydraulic model is performed from WS observables using the variational data assimilation (VDA) algorithm presented in Larnier et al. (2020), with bathymetry-friction patches as in Garambois et al. (2020), following large scale applications with inflows from MGB hydrologic model in Pujol et al. (2020); Malou et al. (2021), to a large and vector of heterogeneous parameters over a complete river network. The principle of this inverse method is to minimize the discrepancy between simulation and observations of river network state dynamics, by adjusting the unknown parameter vector $\boldsymbol{\theta}$ of the hydrodynamic model described in Section 2.1).

2.2.1 Parameter Vector

The parameter vector is composed of spatially distributed parameters of the hydraulic network model, i.e. friction and bathymetry coefficients over the river network and inflow hydrographs at inflow points, and writes as:

$$\boldsymbol{\theta} = \left[\left(Q_{in,u}^0, ..., Q_{in,u}^{T(u)} \right)_{u=1..N_{BC}}; \left(b_{1,s}, ..., b_{N_b(s),s} \right)_{s=1..N_{seg}}; \left(\alpha_s, \beta_s \right)_{s=1..N_{seg}}; \right]^T \tag{9}$$

where $Q_{in,u}^{t=1..T(u)}$ is the upstream discharge hydrograph imposed at N_{BC} main inflow points (upstream BCs) with $T(u)$ discharge values in time (evenly or unevenly discrete hydrograph). The spatialized bathymetry-friction over the river network is as follows: $b_\square$ (resp. $\alpha_\square$ and $\beta_\square$) is the channel bottom elevation (resp. coefficient and exponent of the friction law Eq. 6) with $N_b(s)$ (resp. $N_K(s)$) being the number of bathymetry points (resp. friction patches).

Note that for this study, with the above definition, the friction is assumed spatially uniform by segment of the river network, i.e. a lower spatial density of this control compared to bathymetry ones. This is a consistent hypothesis regarding (i) the rather large meaningful scale of friction parameter in the 1D Manning-Strickler parameterization (ii), and also regarding calibration on nadir altimetry data that are heterogeneous and sparser than model resolution (cf. Garambois et al. (2020); Pujol et al. (2020); Malou et al. (2021)).

The same hypothesis will be used for a parameter estimation experiment with the dense SWOT data in space and time.

2.2.2 Cost function and optimization algorithm

The principle of the VDA algorithm Larnier et al. (2020) is to estimate (discrete) controls of the river network model that minimize the discrepancy between the simulated flow and the available observations. The cost function to be minimized writes:

$$j(\boldsymbol{\theta}) = j_{obs}(\boldsymbol{\theta}) + \gamma j_{reg}(\boldsymbol{\theta}) \tag{10}$$

In this study, flow observations consist in multi-source altimetric data, and the term j_{obs} measures the discrepancy between modelled and observed WS elevations over the hydraulic domain Ω_{hy} such that:

$$j_{obs}(\boldsymbol{\theta}) = \frac{1}{2} \|Z(\boldsymbol{\theta}) - Z^*\|_O^2 \tag{11}$$

The weighted Euclidean norm is defined as $\|x\|_O^2 = x^T O x$, with O an a priori observation covariance operator, simply a diagonal matrix of constant variance σ_o here. The cost function and the regularization (detailed after), both depend on the control parameter $\boldsymbol{\theta}$ through the response of the hydraulic model $\mathcal{M}_{hy}$ (Eq. 4) inflowed by the hydrological model $\mathcal{M}_{rr}$, hence of the full hydrological-hydraulic model $\mathcal{M}$ (Eq. 3) and so $j(\boldsymbol{\theta}) \coloneqq j\left(\mathcal{M}_{\Box}\left(\boldsymbol{\theta}\right)\right)$.

The data assimilation problem reads as the following optimization problem:

$$\hat{\boldsymbol{\theta}} = \underset{\boldsymbol{\theta}}{\operatorname{argmin}} j\left(\boldsymbol{\theta}\right) \tag{12}$$

where $\hat{\boldsymbol{\theta}}$ denotes the analysis we expect to approximate the true control vector $\boldsymbol{\theta}^t$ as closely as possible. This optimization problem, of high-dimension with the composite discharge-bathymetry-friction spatio-temporal parameter vector $\boldsymbol{\theta}$ (Eq. 9) of the hydraulic model $\mathcal{M}_{hy}$, is solved numerically with the L-BFGS algorithm. This quasi-Newton descent algorithm requires, at each step of its iterative process, the gradient of the cost function with respect to the sought parameters, $\nabla_{\boldsymbol{\theta}} j$, that is computed with the adjoint model obtained by automatic differentiation of the forward numerical hydraulic code with Tapenade engine Hascoet & Pascual (2013). Note that hydrological model optimization from hydraulic observables is a very interesting research topic but is not the scope of the present research, see information feedback with adjoint of a differentiable hydrological-hydraulic model in Pujol et al. (2022) or composed adjoint in Huynh et al. (2023, 2024). See VDA concepts in Monnier (2021) and references therein.

The control vector $\boldsymbol{\theta}$ sought from WS observables only contains parameters of different nature that trigger indiscernible signatures in the simulated WS, hence the inverse problem is ill-posed (see analysis in Garambois et al. (2020); Larnier et al. (2020) on model structural and spatial equifinality). Therefore it is regularized as detailed in C1.

The background $\boldsymbol{\theta}^{(0)}$ on the sought parameters is simply obtained in this study by inverting the hydraulic model in steady state assuming a geometry shape and friction value, given inflows provided by a precalibrated hydrological model, which is detailed in numerical experiment design and discussed later.

The VDA algorithm is schematized in Figure 1 with its main components and data fluxes.

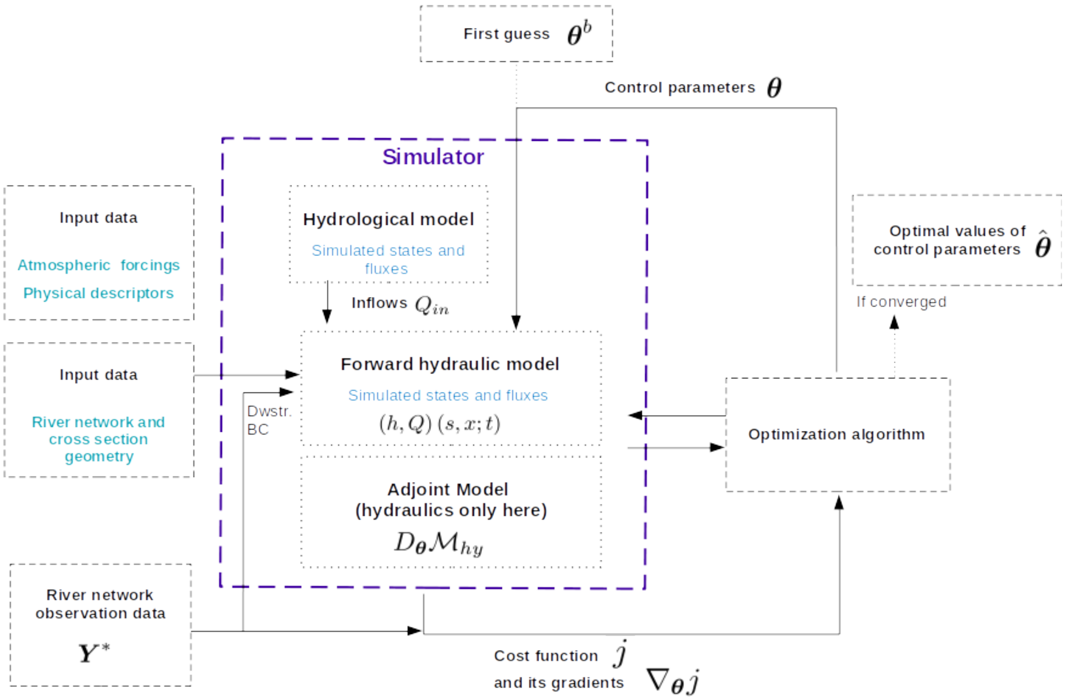

Figure 1. Diagram of the adjoint-based variational data assimilation (VDA) algorithm (inspired from principle in Monnier (2021)).

3 Case, data and processing algorithms

This study focuses on the Maroni basin (Figure 2), in French Guiana, under the influence of a tropical climate with marked rainy and dryer seasons, and is based on a diverse and rich dataset feeding the different components of the forward hydrological-hydraulic model and the VDA algorithm as follows:

- **Hydrological modeling** (MGB): physical basin descriptors for semi-distributed mesh of the basin and a priori parameters constrains and hydrometeorological data from worldwide open databases for model setup, discharge at in situ gauges for its calibration (seedetail in subsection 3.3.1).
- **Hydraulic modeling** (DassFlow1D): A priori river network database and multi-satellite dataset of WSE (ICESat2) and WSW (Sentinel) profiles for model geometry construction, inflow discharge from the hydrological model for a priori bathymetry estimation (see section 3.3).
- **Variational Data Assimilation**: WSE data from Multi-satellites (Sentinel 3, ICESat2, SWOT) an in situ (georeferenced gauges).

This section details the automatic processing algorithms taking as input open databases and multi-satellite data for:

- Extracting WS elevations Z^* and width W^* respectively from altimetric data, drifting (ICESat-2) or not (Sentinel 3) and water masks (either optical or radar),
- Hydraulic model meshing,

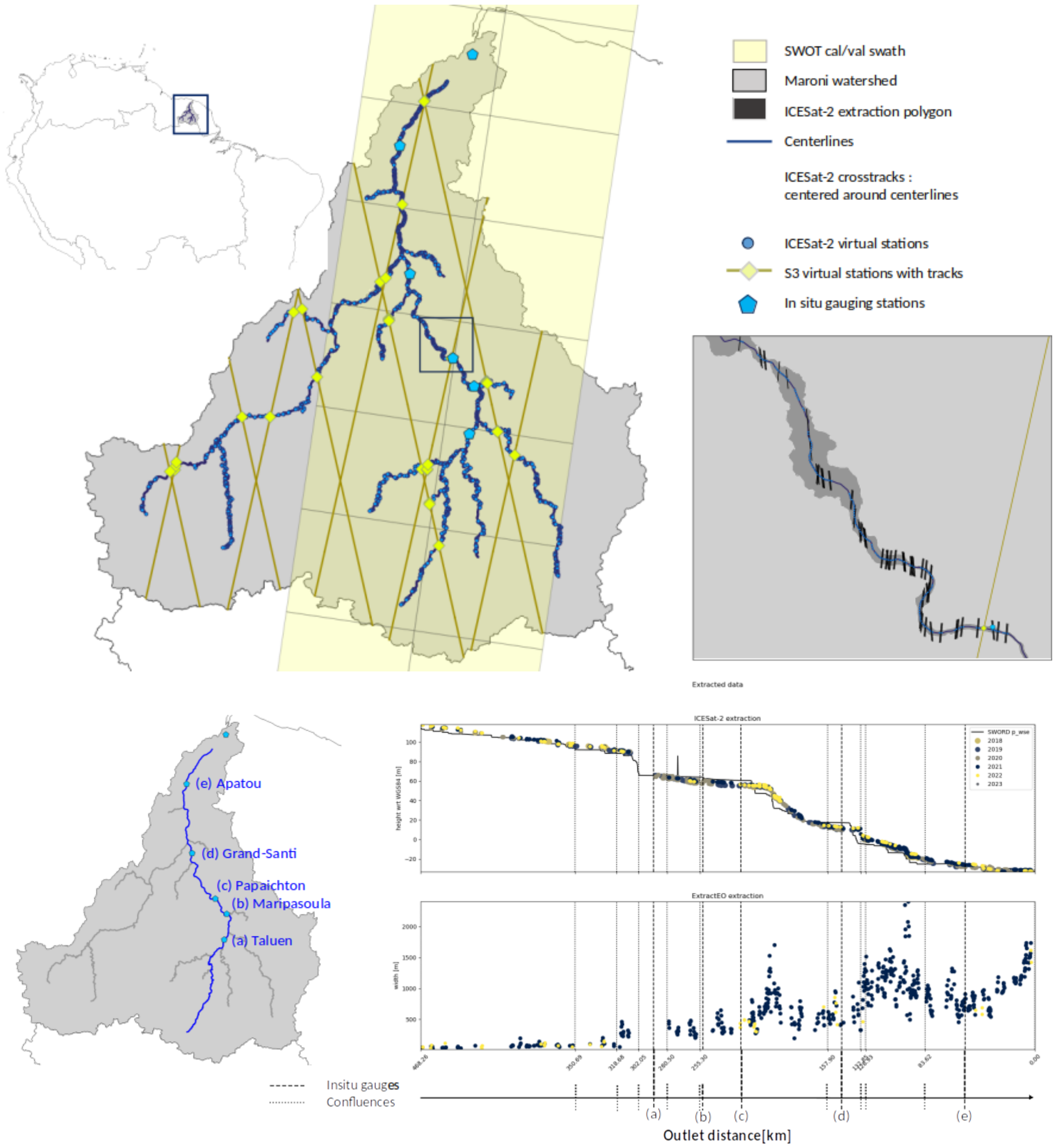

Figure 2. The Maroni River basin in French Guiana with (top) multi-satellite and in situ flow observability, (Bottom) main river water surface profile from drifting nadir altimetry (ICESat-2).

- Coupling to hydrological model.
- Wavelet-based filtering algorithm for SWOT 1D river surface elevation product.

3.1 WSE and WSW processing from nadir altimetry and radar images

Water surface elevation (WSE) data are obtained from already processed Sentinel 3 data at virtual station (VS) but originally here also from drifting ICESat-2 ATL13 data with a proposed processing chain. This chain uses an a priori water mask, and aims to provide hydraulically consistent WSE on XS lines over the vectorial river network shapefile, and is summarized in Figure 3 and detailed in appendix B3.

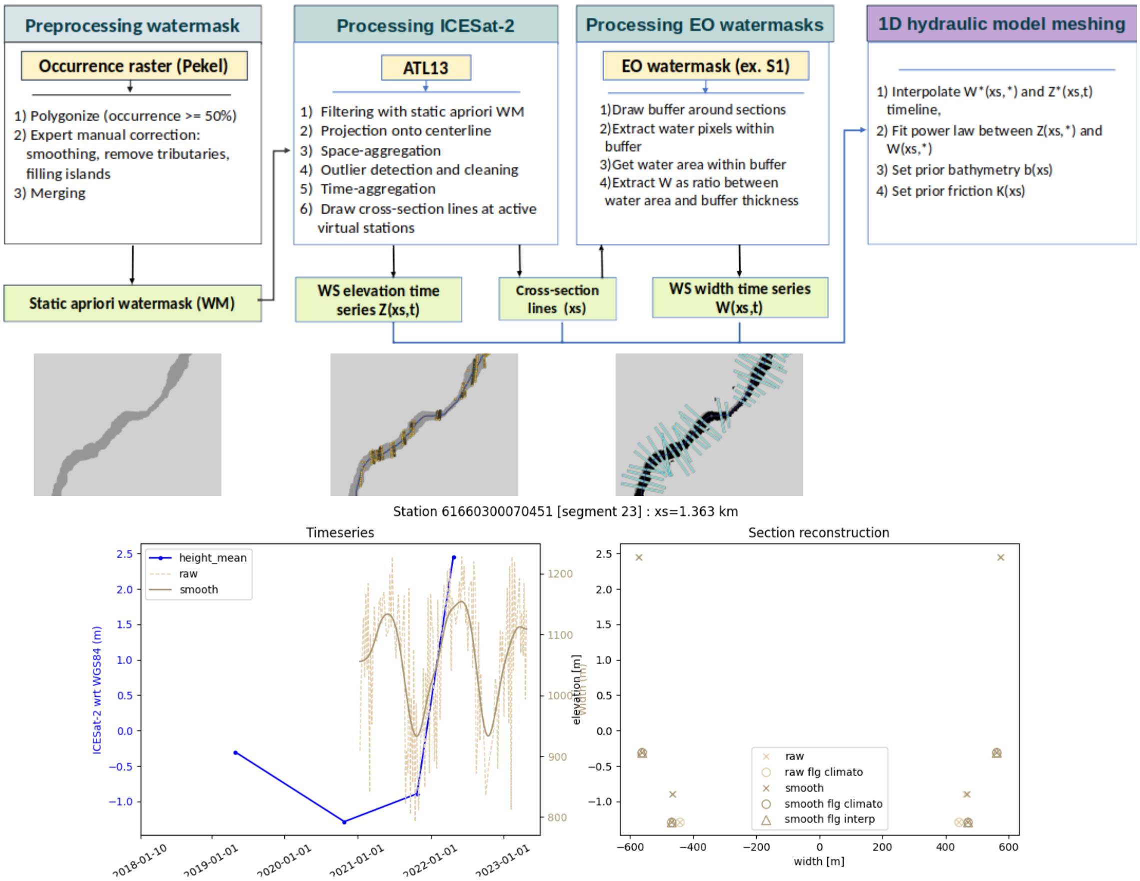

Figure 3. Flowchart of the processing chain for water masks and ICESat2 data, 1D hydraulic model meshing (Top and middle). Example of obtained WS elevation and width time series (Bottom).

Water surface width (WSW) data are obtained from dynamic water masks, i.e. varying water masks at different times and flow conditions, using the ExtractEO tool from ICube-SERTIT applied to Sentinel-1 radar images which are accurate and freely available worldwide **(verifier/corriger)** (cf. Appendix C). These widths are also usable for non rectangular XS parameterization but a simple rectangular XS is sufficient for this study on the Maroni as explained after. Complex XSs have been determined on the Niger basin and a fairly satisfying model setup (not presented here and left for further research). Note that the vertical referencing of those dynamic water extents in time can be performed with altimetric measurements around image acquisition date - simultaneous WSE and WSW measurement with SWOT.

This multi-satellite data preprocessing chain is used to provide inputs to an automatic pre-processing algorithm for building coupled hydrological-hydraulic model setup and adapted to MGB and DassFlow1D in particular.

The obtained hydraulic mesh granularity is visible on Figure 2 and XS width represented on the Maroni main stream in Figure 5 (bottom, in yellow). Note the choice made for WSW, which is a crucial quantity to determine a hydraulic model geometry in absence of reliable bathymetry data, to use Sentinel data which are relatively accurate. This should benefit to information extraction from the unprecedented WSE data from SWOT. Detailed steps of this algorithm are given in Section A.

3.2 Dedicated SWOT data filtering-segmentation algorithm

The very new and unprecedented SWOT data provides astonishing hydraulic visibility over worldwide rivers from our first analysis yet contains, as expected, some measurement errors that can locally be quite large. Dealing with the SWOT L2 RiverSP product in this article, i.e. WSE along river centerlines at a fine spatial resolution of 200m (node scale), we apply a wavelet-based filtering/segmentation algorithm based on our previous work with synthetic data Montazem et al. (2019).

The wavelet-based filtering and segmentation algorithm, that is adapted to process WSE longitudinal profiles such as those provided by SWOT or by in situ GNSS while preserving the WS signatures of hydraulic controls (HCs), is based on the approach and Matlab codes of Montazem et al. (2019). The idea, since hydraulic variability appears in the WS signal of interest at multiple spatial scales, is to use wavelet processing to isolate the signatures of local hydraulic controls (HCs). The use of a wavelet basis makes it possible to decompose profiles of free-surface spatial WSE signals, with very good accuracy, while retaining localised frequency information. One original feature is the use of wavelets to both denoise and segment signals in a consistent space-frequency localized way. This approach introduces very few oscillations into the reconstructed filtered signal and is suitable for unsteady signals and the detection of strong curvature signals. This algorithm is called pyrscwt (Python River Segmentation with Continuous Wavelet Transform) and is based on a custom implementation in Python of a continuous wavelet transform leading to accurate 1D signal projections and reconstructions.

SWOT 1-day orbit data filtering with the wavelet based algorithm are presented in Figure 4. This algorithm enables to efficiently retain the main outliers (red points) as evidenced on the graph, while perceiving hydraulic information.

3.3 Maroni model construction

3.3.1 Meshing and hydrological-hydraulic coupling

First, the hydraulic domain Ω_{rr} is determined using the river centerlines from SWORD database. It stops downstream at Apatou, at a point that is disconnected from tidal influence because of a sharp river channel bottom variation. Upstream limits are set as rivers draining more than $1500km^2$ using drainage area obtained from DEM processing. Thus the hydraulic model covers a long portion of the Maroni main course and a significant number of tributaries.

Once the hydraulic river network domain Ω_{hy} is determined, we can straightforwardly identify the upstream inflow points, here $N_{BC} = 12$, where hydrological model discharge applies as BC for the 1D hydraulic model resolution. The lateral inflow points are determined such that $N_{lat} = 181$ here.

The hydrological model $\mathcal{M}_{rr}$ is the MGB semi-distributed model well adapted for this tropical basin. Classical preprocessing was applied to obtain flow directions and accumulations based on MERIT-Hydro DEM (Yamazaki et al. (2019)), following Pontes et al. (2017) steps. Spatial hydrological response unit (HRU) descriptors on soil and vegetation were taken from FAO HWSD (Nachtergaele et al. (2023)) and ESA WorldCover (Zanaga et al.

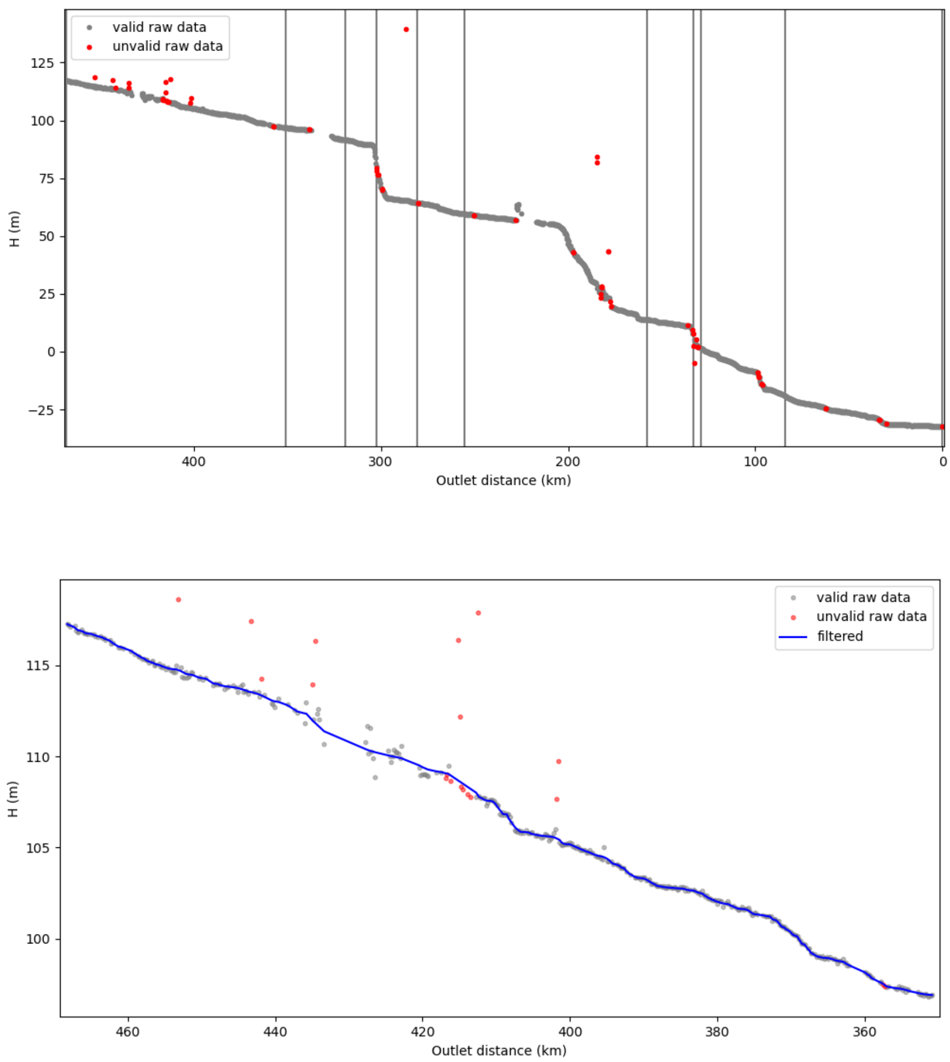

Figure 4. Hydraulic filtering of SWOT L2-RiverSP products at node scale on the main stem for cycle 569 with pyrscwt algorithm (Python River Segmentation with Continuous Wavelet Transform). (Top) Complete main stem, (bottom) zoom on upstream segment of the main stem which shows the filtered profile in blue solid line.

(2021)), respectively, converted into 12 HRUs of distinct flow-generation potential. Hydro-meteorological forcings (climate, rainfall) are taken from ECMWF ERA5 dataset and GSMAP-RT real-time product (Kubota et al. (2020)). MGB is calibrated by hand on in situ discharge data with low parameters spatialization: the Maroni River basin is divided into 10 sub-basins corresponding to the main tributaries, namely the Litani, Tampok, Grand Inini, Lawa, Gonini, Upper Tapanahoni, Palumeu, Tapanahoni, Abounami and Maroni. Calibration is performed using observed discharge from SCHAPI https://www.hydro.eaufrance.fr/ (last access on 2024-05-25) at 5 gauges (namely Lawa at Taluen, Tampok at Degrad-Roche, Lawa at Maripasoula, Maroni at Grand-Santi and Maroni at Langa-Tabiki, see Figure 2) on the period going from 2016 to 2023. Calibration is carried from upstream to downstream, and ungauged basins are calibrated using the nearest downstream gauge. The discharge simulated by the semi-distributed hydrological model are used to feed the hydraulic model at its upstream and lateral inflow boundaries defined above.

The hydraulic mesh and coupling points are represented in Figure 5 along with the longitudinal bathymetry profile of the hydraulic model and a simulated flow line on the main stream of the Maroni River - over which 1-day orbit SWOT data will be assimilated after - highlighting succession of marked riffles/jumps corresponding to hard rock outcrops. This results in a complex longitudinal bathymetry gradient, in a addition to complex width variability and anastomosed reaches, that translate in complex WS variabilities representing a challenging measurement case for SWOT.

3.3.2 Hydraulic model geometry

The geometry of modeled reaches of the river network is automatically determined from the multi-satellite dataset composed of spatio-temporal water extents and flow lines: Sentinel WSW and a subset of ICESat2 WSE profiles, the remaining part of ICESat2 and SWOT WSE data being kept for DA experiments.

The XS geometry of the hydraulic model is simply defined as rectangular, using the median WSW over the dynamic water masks available in our dataset that have been extracted from Sentinel radar images with ExtractEO algorithm. Using a rectangular hydraulic XS on the Maroni is a reasonable hypothesis for this river showing relatively reduced extent variations as done for the "nearby" also anastomosed Negro River in Pujol et al. (2020); Malou et al. (2021) (cf. Subsection 2.1.4), and also as shown by the satisfying hydraulic modeling results obtained in what follows.

The background (a priori) river bed elevation $b^{(0)}(s,x)$ of the hydraulic model $\mathcal{M}_{hy}$ is determined as follows:

- Constant in time WSW W^* are obtained from images processing (median water mask over the period 2019-2021 from Sentinel-based water masks).
- XS shape is assumed rectangular and friction is assumed to be spatially uniform with $K^{(0)} = 30 \ \left[\mathrm{m}^{1/3}.\mathrm{s}^{-1}\right]$,
- Inflows ($Q_{in,i=1..N_{BC}}$ and $q_{lat,i=1..N_{lat}}(t)$) are assumed to be the median discharge over the studied period ($Q_{in}^{*,50}$ and $q_{lat}^{*,50}$) provided by the pre-calibrated hydrological model.

Then, the hydraulic model is run in steady state and the background bathymetry $b^{(0)}(s,x)$ is obtained by inverting from a modeled median flow line $Z^{*,50}$ using altimetric data. The hydrological-hydraulic model mesh is schematized in Figure 5.

Note that our modelling chain enables using a more complex geometry, with a rectangle for wet bathymetry plus a superimposition of trapeziums from dynamic water masks, is possible with our algorithm and will be studied in further research along with wet bathymetry parameterizations from S. L. Dingman (2007); S. L. Dingman & Afshari (2018) as used at reach scale in Andreadis et al. (2020).

3.4 Numerical experiments design

The Multi-satellite data assimilation experiments, with the VDA algorithm applied to the coupled hydrological-hydraulic model $\mathcal{M}$ (cf. section 2), aims to show the potential of estimation at river network scale of inflow discharges, bathymetry and friction of the hydraulic model. The sought parameter vector $\boldsymbol{\theta}$ of the hydraulic model $\mathcal{M}_{hy}$ is composed of $Q_{in,u=1..N_{BC}}^{t=1..T(u)}$ hydrographs at $N_{BC} = 12$ inflows, bathymetry b at $N_b = 2572$ points and friction coefficients α and β at $N_K = 24$ friction patches (i.e. spatially uniform segments). For each DA experiment, the same median WS width W^* is used to define section geometry over the river network, but the first guess on bathymetry $b^{(0)}$ are different since they are computed for different periods from different median inflow discharges and median altimetric flow lines $Z^{*,50}$ with the method explained before. The numerical experiment plan, consisting in assimilating more or less sparse data cocktails to infer the above defined parameter vector, is as follows:

1. **"NadAlti.4limni"**: Nadir altimetry, drifting IceSat2 and fixed S3 VS, plus 4 in situ WS elevation time series at Maripasoula, Papaichton, Grand Santi and Apatou gauges (with a WGS84 vertical reference in coherence with altimetry), over the period 2019/01/01 - 2019/03/31; (hence b is optimized at those in situ gauges locations); prior bathymetry is $b^{(0)}_{N4l}$.
2. **"SWOT only"**: 1-day SWOT orbit data only assimilated over the period 2023/05/15 to 2023/07/10 (Number of WSE space-time points: Altimetry (ICESat2+S3): 284, in situ: 8644, total(ALTI+in-situ): 8928); prior bathymetry is $b^{(0)}_{SWOT}$.

These VDA experiments, started from a prior $\boldsymbol{\theta}^{(0)} = \left(Q_{in,u=1..N_{BC}}^{*,t=1..T(u)},\, b^{(0)}_{\square}, K^* = 30\right)$ with inflows from MGB hydrological model, will study the constraining power of classical nadir or wide swath SWOT altimetry to constrain a hydraulic model of a poorly gauged basin built from remote sensing data. Particular attention will be paid to the potential of estimation of spatialized channel parameters and inflow hydrographs.

Note that all those inference scenarios correspond to a quasi-ungauged setup for the inversions over the hydraulic network, i.e. without considering in situ discharge information within the studied hydraulic domain Ω_{hy}, and only indirectly at its boundaries. Indeed, discharge data at in situ gauges within Ω_{hy} were only used for the pre-calibration of the hydrological model that provides a priori hydrographs at inflow BCs and median discharge in time is used to determine a priori hydraulic bathymetry.

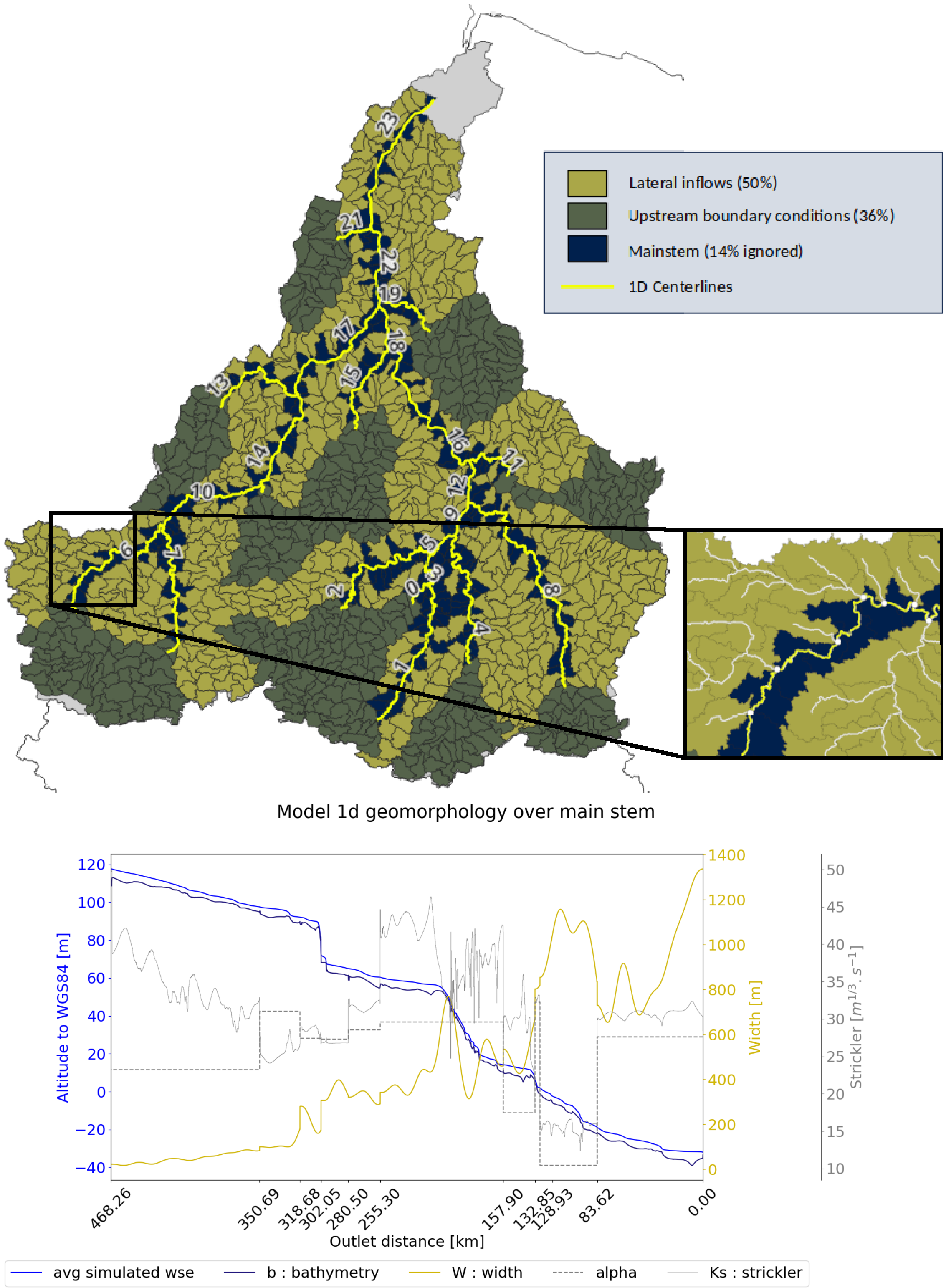

Figure 5. Hydrological-hydraulic mesh with inflow points (Top) and simulated flow line profile on the Maroni main stream after assimilation of SWOT 1 day data (VDA experiment "SWOT only"), calibrated bathymetry and friction profiles $\hat{b}(s,x)$ and $\hat{K}(s,x,\overline{h}) = \hat{\alpha}\overline{h}^{\hat{\beta}}(s,x)$ for successive connected segments $s = (1,3,5,9,12,16,18,22,23)$ with $\overline{h}(s,x)$ the average flow line on the studied SWOT time window (Bottom).

For every experiments, the parameters of the background error covariance matrix are set as follows: $\left(\sigma_{Q_{in,i}} = 0.01\bar{Q}^{(0)}_{in,i}\right)$, $L_Q = 10days$, $\sigma_b = 0.1m$, $L_b = 200m$, $\sigma_\alpha = 0.5m^{1/3}.s^{-1}$ and $\sigma_\beta = 0.01$.

4 Results and discussions

The overall performances, in terms of fit to the WSE data used in calibration, and also of reproduction of discharge at gauging stations inside the hydraulic domain Ω_{hy} (not used in assimilation) is very satisfying for both VDA experiments. A very significant fit improvement to observed WSE over the spatio-temporal domain, below 0.5m (improvement of fit to WSE from prior is of 54% for "NadAlti.4limni" and 69% for "SWOT only" which is far denser). Very satisfying performances in terms of simulated discharges at validation gauges within the river network is obtained: significant improvement of discharge of 43% for "NadAlti.4limni" (Figure 4.1) and 37% for SWOT (Figure 10) from prior. Note that those experiments are performed on different time periods, hence for different hydrological responses and prior $\boldsymbol{\theta}^{(0)}_{\square}$.

In the following, the results of DA experiments "NadAlti.4limni" and "SWOT only" are analyzed into more details, in terms of fit to the observations, of validation on discharge gauges and also in terms of correction on the hydraulic parameters inferred.

4.1 Multimission nadir altimetry and in situ WSE assimilation (NadAlti.4limni)

The assimilation experiment "NadAlti.4limni", of S3 and ICESat2 nadir altimetry along with in situ WSE at the 4 in situ gauges is analyzed here.

The cost function minimization and its gradients to the sought spatialized parameters are presented in Figure 6 along with the fit to WSE data of the model before calibration $\mathcal{M}(\boldsymbol{\theta}^{(0)}_{N4l})$ and after $\mathcal{M}(\hat{\boldsymbol{\theta}})$. The fit of WSE is significantly improved from background prior parameters $\boldsymbol{\theta}^{(0)}_{N4l}$ to the control $\hat{\boldsymbol{\theta}}$ estimated by VDA of WSE, with a simulation error on WSE at 87% in [-0.5, 0.5]m, at 64% in [-0.25, 0.25]m, error for $5-th$ (resp. $95-th$) quantile $\epsilon_{Q5} = -0.6$m, (resp. $\epsilon_{Q95} = 0.48$m). This represents a significant improvement of the fit to the spatio-temporally heterogeneous WSE used in calibration. Interestingly, this also results in a significant improvement of the discharge simulated at gauging stations (discharge not used in this calibration but only WSE of four out five gauges, gauge section bathymetry is inferred) within the hydraulic domain Ω_{hy} as evidenced by Figure 4.1 (final NRMSE between 0.08 and 0.19), which were not used in calibration but only WSE at those gauges in addition to nadir altimetry data over the network (see VS locations on Figure 2). Indeed, the data assimilated in "NadAlti.4limni" consist in relatively sparse WSE over the spatio-temporal domain (295 satellite altimetry points over the network) with some temporal density provided by WSE at the four gauges (2161 WSE values per gauge hence 8644), compared to the size of the sought spatio-temporal controls. Internal discharge prediction is improved after assimilation of WSE, compared to the prior hydraulic model, at all gauges which are located along the Maroni main stream. This improvement results from the correction of hydraulic model controls which pertain to spatialized channel bathymetry-friction and hydrographs at $N_{BC} = 12$ upstream inflow BCs.

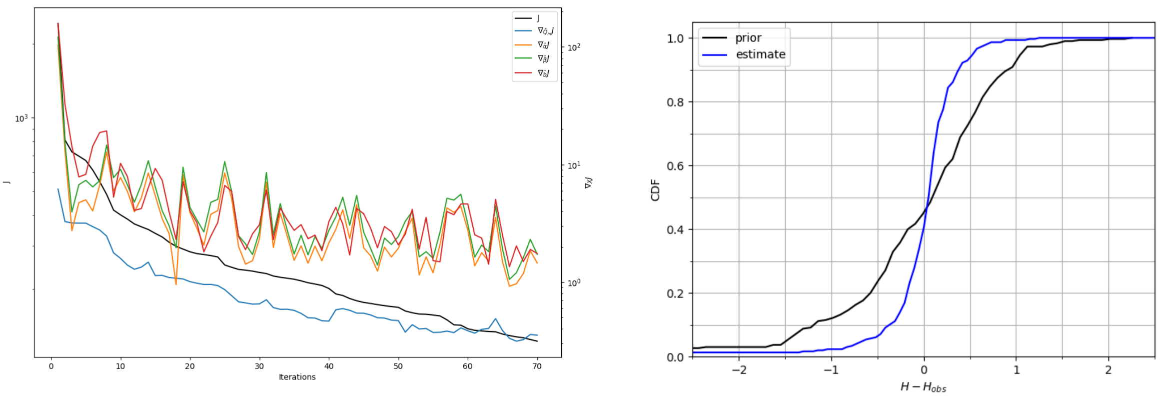

Figure 6. "NadAlti.4limni" data assimilation experiment convergence. (Left) Convergence curve with cost J and its gradients $\nabla_\square$ w.r.t to the sought spatially distributed inflows discharges Q_{in}, friction parameters α and β, bathymetry b. (Right) cumulative distribution function (CDF) of absolute misfit of simulated WSE to altimetry data in meters, "prior" is with background parameters $\boldsymbol{\theta}^{(0)}_{N4l}$ and "estimate" is with the calibrated $\hat{\boldsymbol{\theta}}$. Over 295 space time points at nadir altimetry VS and in situ gauges model misfit values are as follows: 87% in [-0.5, 0.5]m, 64% in [-0.25, 0.25]m, error for $5-th$ (resp. $95-th$) quantile $\epsilon_{Q5}=-0.6$m, (resp. $\epsilon_{Q95}=0.48$m). RMSE on Z is 0.36m (prior:0.8m).

Those satellite-based estimates of mass fluxes and river network bathymetry-friction parameters $\hat{\boldsymbol{\theta}}_{N4l}$, at the upstream boundaries Γ_{up} and over the river network hydraulic domain Ω_{hy} are summarized in Figure 11. For most segments of the river network, significant corrections of bathymetry-friction are obtained, that along with upstream inflow corrections (see inferred inflows hydrographs and bathymetry profiles in appendix D), enable the improvement of the fit of simulated flow line to local altimetry and in situ WSE data. Note that the contribution of those hydraulic parameters to the simulated flow line is complex because of (i) upstream to downstream propagation and aggregation of the inflow discharges along the river network, only upstream BCs on Γ_{up} are corrected here (representing 50% of basin area as shown by Figure 5), (ii) of local competition between bathymetry and friction embedded into the friction source term S_f of the 1D Saint-Venant model (cf. Equation 4) and (iii) of the complex correlated influence of those hydraulic controls towards upstream on so called backwater length under the fluvial regime studied (see Samuels (1989); Montazem et al. (2019)). In other words, the studied inverse problem, that is estimating most flow controls (except lateral inflows) of the 1D Saint Venant model, is very difficult and faced with local equifinality and spatial equifinality and it has been possible to find a satisfying solution thanks to a realistic prior on the sought parameters and thanks to the regularizations introduced via covariances matrices (cf. section 2.2.2). A finer hydraulic analysis of local hydraulic controls inferred is made after, along with a discussion on the controllability of hydrological inflows.

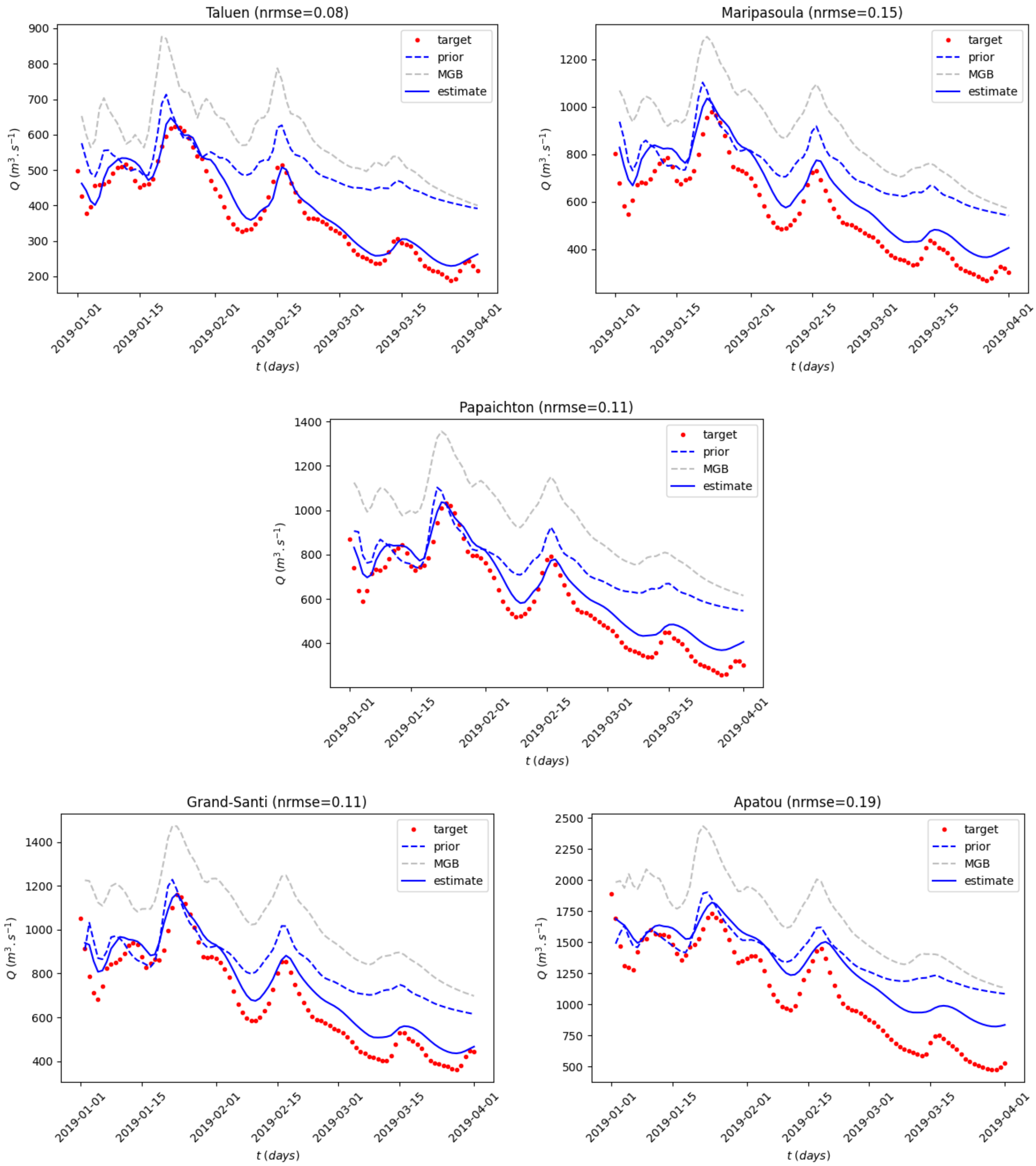

Figure 7. Validation of simulated discharge at the available gauges along the Maroni main stream after assimilation ("NadAlti.4limni") of nadir altimetry (Sentinel 3 and ICESat-2) and in situ WSE at those gauges except Taluen. Multi-gauge RMSE on Q is 143.4m3/s (prior: 252.6m3/s).

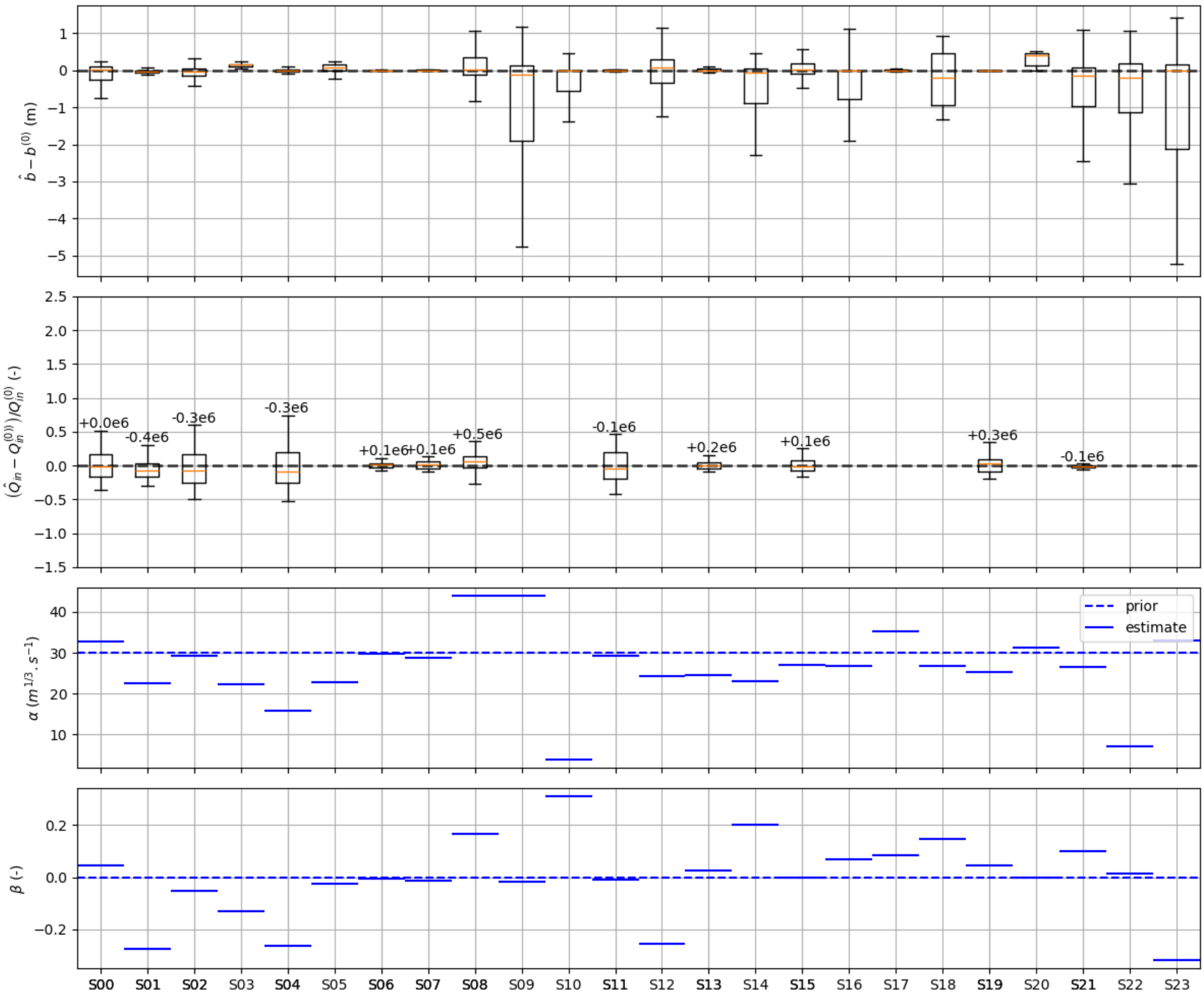

Figure 8. Model parameters $\hat{\boldsymbol{\theta}}$ inferred by VDA in the "NadAlti.4limni" experiment from background (prior) parameters $\boldsymbol{\theta}_{N4l}^{(0)}$ represented by segment of the river network "S00" to "S23": boxplots of spatially distributed corrections (top) of bathymetry $b(s,x)$ at $N_b = 2572$ hydraulic cross sections and of (second) inflow discharge hydrographs $Q_{in,u=1..N_{BC}}^{t=1..T(u)}$ at $N_{BC} = 12$ inflows,(third and fourth) friction parameters $\hat{\alpha}$ and $\hat{\beta}$ over the 24 segments composing the simulated river network.

4.2 SWOT 1-day only data assimilation

The assimilation experiment of "SWOT only" wide swath altimetry data, track #007 during fast sampling (cal-val) orbit covering a large area of the Maroni basin including the main stream "along track" with 1 day repetitivity, is analyzed here. This time period from may to august 2023, covered by SWOT 1 day data, corresponds to peak and declining limb of a relatively strong flood: the estimated peak flow in May 2023 at Apatou downstream of the basin is above 4500 m^3/s. Note that the wavelet-based filtering algorithm is systematically used to remove outliers (cf. Figure 4) before VDA.

The cost function minimization and its gradients to the sought spatialized parameters are presented in Figure 9 along with the fit to WSE data of the model before calibration $\mathcal{M}(\boldsymbol{\theta}^{(0)}_{SWOT})$ and after $\mathcal{M}(\hat{\boldsymbol{\theta}})$. The fit of WSE is significantly improved from background prior parameters $\boldsymbol{\theta}^{(0)}_{SWOT}$ to the control $\hat{\boldsymbol{\theta}}$ estimated by VDA of WSE, this time over much more space-time points of WSE (179,192 with "SWOT only" over a shorter period compared to 295 points in "NadAlti.4limni"!), with a simulation error on WSE at 86% in [-0.5, 0.5]m, at 63% in [-0.25, 0.25]m, error for $5-th$ (resp. $95-th$) quantile $\epsilon_{Q5} = -0.6$m, (resp. $\epsilon_{Q95} = 0.48$m). This represents a significant improvement of the fit to SWOT WSE used in calibration, that are 600 times denser in space and time than nadir altimetry and in situ data previously used.

Interestingly, over the shorter time window studied here and this assimilation of SWOT data only results in an improvement of the discharge simulated at gauging stations (unseen data) within the hydraulic domain Ω_{hy} (cf. Figure 10). The nrmse on discharge at those internal gauges range between 0.11 and 0.26 which is a fairly good result, especially for this inference in the declining limb of a strong flood not reproduced by the hydrological model (grey dashed hydrographs) hence providing unfavourable prior inflows for VDA (blue dashed hydrographs simulated by $\mathcal{M}\left(\boldsymbol{\theta}^{(0)}_{SWOT}\right)$).

The optimized parameter $\hat{\boldsymbol{\theta}}_{SWOT}$, i.e. inflow discharge hydrographs, spatialized bathymetry and friction over the river network hydraulic domain are summarized in Figure 11. Again, for most segments of the river network, substantial corrections of bathymetry-friction are obtained, that along with upstream inflow corrections, enable the improvement of the fit of simulated flow to local altimetry and in situ WSE data. Recall that the inference from WSE of those parameters, i.e. all controls of a 1D Saint-Venant hydraulic model, that have a correlated influence on WS remains faced to local structural equifinality (due to parameters embedded into friction term S_f) but also to spatial equifinality (, see analysis in Garambois & Monnier (2015); Garambois et al. (2020); Larnier et al. (2020); Pujol et al. (2024)). That is why covariance matrices are used in the VDA algorithm (as for previous "NadAlti.4limni" esperiment) to obtain a regularizing effect of this ill-posed inverse problem, through a preconditioning effect and a spatial or temporal regularization effect (smoothing of estimated spatial or temporal quantities when denser than observations). The inferred hydrographs and bathymetry profiles of each segments of the network are shown in appendix D. Detailed spatial parameters variabilities can be inferred thanks to the spatial density of SWOT data which analyzed after compared to the inference with the nadir altimetry WSE.

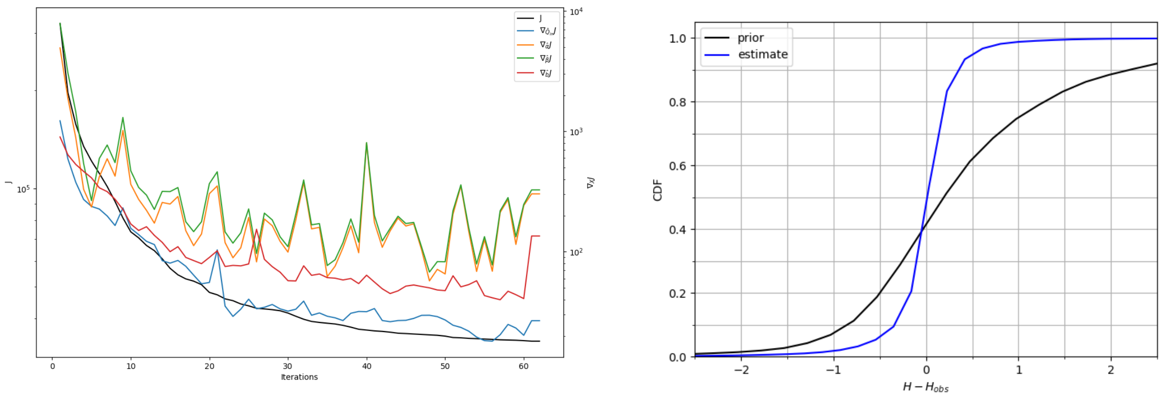

Figure 9. "SWOT only" data assimilation experiment convergence. (Left) Convergence curve with cost J and its gradients $\nabla_{\square}$ w.r.t the sought spatially distributed inflows discharges Q, friction parameters α and β, bathymetry b. (Right) cumulative distribution function (CDF) of absolute misfit of simulated WSE to altimetry data in meters, "prior" is with background parameters $\boldsymbol{\theta}^{(0)}_{SWOT}$ and "estimate" is with the calibrated $\hat{\boldsymbol{\theta}}$. Over 179192 space time points at SWOT L2 RiverSP product at node scale over the river observed part of the river network, model misfit values are as follows: 86% in [-0.5, 0.5]m, 63% in [-0.25, 0.25]m, error for $5-th$ (resp. $95-th$) quantile $\epsilon_{Q5} = -0.7$m, (resp. $\epsilon_{Q95} = 0.55$m).

4.3 Detailed analysis of inferred parameters

The inferences of spatio-temporal parameters of the river network hydraulic model have been performed from 2 datasets with significantly different spatio-temporal density, SWOT one being much denser in space and time. The bathymetry-friction profiles inferred over the Maroni main stream, i.e. the river network segments $s = (1, 3, 5, 9, 12, 16, 18, 22, 23)$ in Fig.5, with WSE from nadir altimetry and gauges or SWOT only are compared in Figure 12.

Both assimilation experiments "NadAlti.4limni" and "SWOT only" lead to the inference of spatially distributed bathymetry-friction over the network, along with upstream inflows correction. Recall that those estimations are performed from different priors, either $\boldsymbol{\theta}^{(0)}_{N4l}$ or $\boldsymbol{\theta}^{(0)}_{SWOT}$, in terms of median discharge used to infer prior bathymetry as explained before. Both experiments are performed with identical setup for covariance matrices, for weights $\sigma_{\square}$ and correlation length $L_{\square}$. Those inferred parameters of the hydraulic model are optimal solutions of the inverse problem (Equation 12) given the WSE data considered, i.e. effective bathymetry-friction-inflows enabling the best fit to the WSE data considered.

The calibrated hydraulic models obtained can be used to derive stage-fall-discharge laws for operational discharge forecasting using SWOT WSE and WS slopes (cf. Malou et al. (2021)). Such a network scale hydrological-hydraulic model is also relevant for studying potential upgrades of "reach scale" SWOT discharge algorithms, such as HiVDI Larnier et al. (2020), that would benefit for a better constraint of the double regionalization problem of uncertain or unknown spatio-temporal hydrological and hydraulic parameters from sparse data.

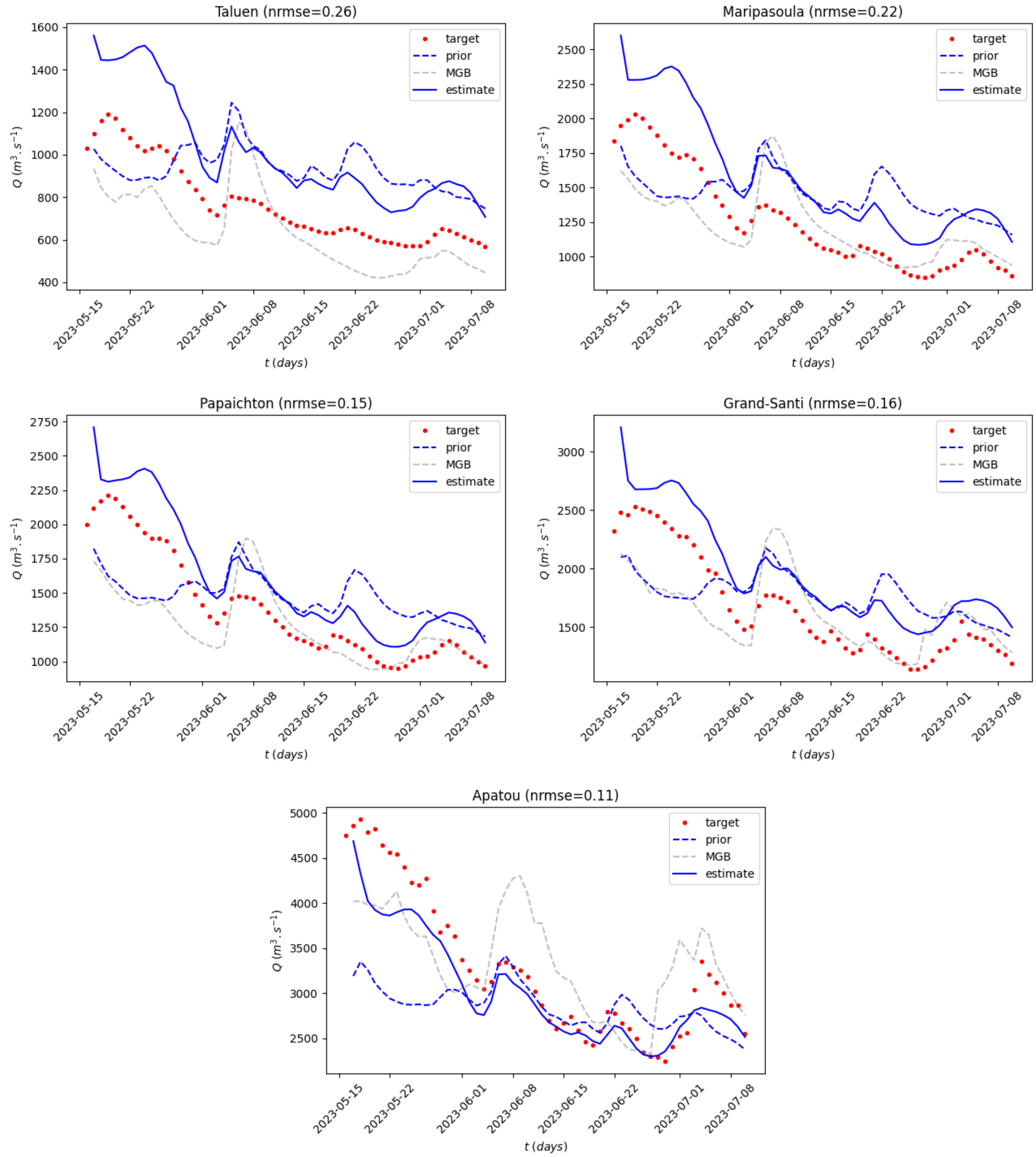

Figure 10. Validation of simulated discharge at the four available gauges along the Maroni main stream after assimilation of SWOT 1day altimetry over the Maroni Network. Multi-gauge RMSE on discharge is 312.5m3/s (prior: 497.55m3/s).

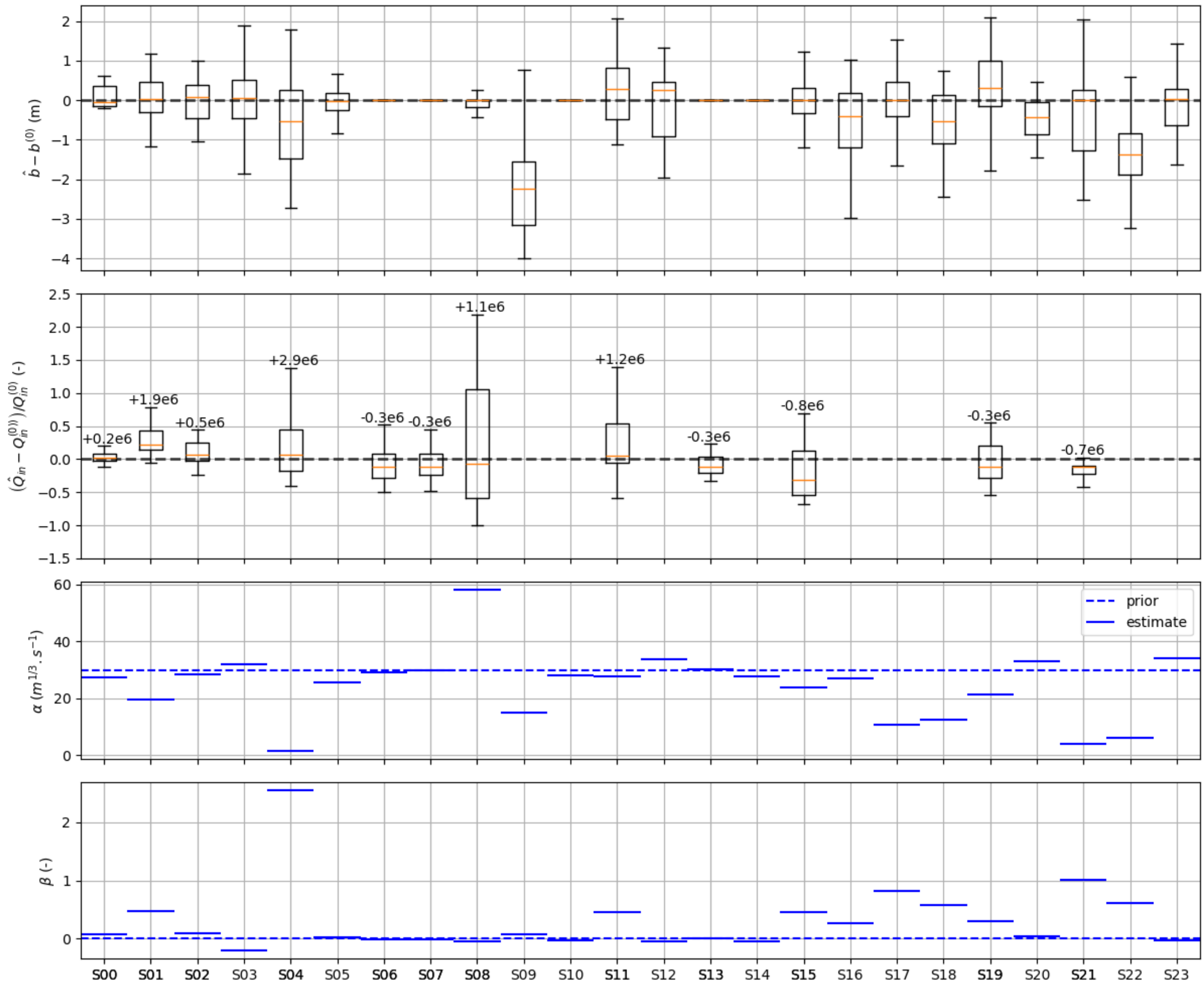

Figure 11. Model parameters $\hat{\boldsymbol{\theta}}$ inferred by VDA in the "SWOT only" experiment from background (prior) parameters $\boldsymbol{\theta}^{(0)}_{SWOT}$ represented by segment of the river network "S00" to "S23": boxplots of spatially distributed corrections (top) of bathymetry $b(s,x)$ at $N_b = 2572$ hydraulic cross sections and of (second) inflow discharge hydrographs $Q_{in,u=1..N_{BC}}^{t=1..T(u)}$ at $N_{BC} = 12$ inflows,(third and fourth) friction parameters $\hat{\alpha}$ and $\hat{\beta}$ over the 24 segments composing the simulated river network.

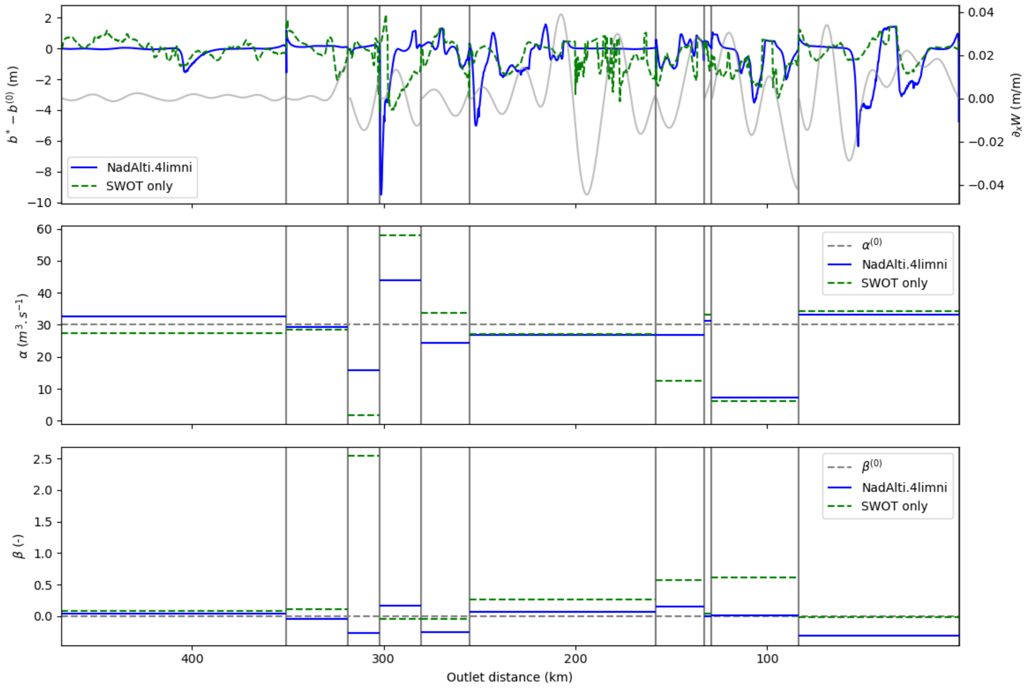

Figure 12. Longitudinal profiles along the Maroni main stream, segments $s = (1, 3, 5, 9, 12, 16, 18, 22, 23)$, of innovation after VDA on bathymetry and friction parameters along with channel width.

Both assimilation experiments, given the same channel width data W^*, lead to infer non-trivial channel hydraulic controls (cf. definition in Montazem et al. (2019)) as depicted by Figure 12 and on flow profiles by segment in appendix D), that enable to produce more realistic WS signatures w.r.t the assimilated WSE in the sense of the observation cost function. More spatial variations are obtained on the bathymetry inferred with the denser SWOT data.

Regarding inflow correction, only upstream inflows, that correspond to 50% of the basin drainage area, were considered in this study. The inference of the remaining numerous lateral flows, of various magnitudes depending on their corresponding drainage area, is a difficult issue (cf. Pujol et al. (2020) with analysis of frequential identifiability of inflows, see also Brisset et al. (2018)) and should be studied in further research. The transposability of the hydraulic parameters obtained with our VDA approach would be possible and coherent if they were calibrated simultaneously with hydrological model parameters - that could be used in temporal extrapolation. More generally, this pertains to the difficult issue of joint optimization of spatio-temporally distributed parameters of a hydrological-hydraulic model. This would be feasible with the present VDA approach applied to a differentiable hydrological-hydraulic solver as proposed in Pujol et al. (2022). Such approaches would also benefit from differentiable regionalization schemes included into the forward model to map physical descriptors onto model parameters as done with a regionalization neural network in Huynh et al. (2023) or even a learnable spatially distributed hydrological model on top of a differentiable hydraulic model (Huynh et al., 2024).

5 Conclusion

This article newly studied the improvement of integrated hydrological-hydraulic (H&H) models, of a river network within its basin, by leveraging the unprecedented hydraulic visibility from the recently launched SWOT satellite in complement of altimetry and imagery from other state-of-the-art satellites used to build the prior model geometry. It is the first application of VDA over a differentiable river network hydraulic model fed by a semi-distributed hydrological model over a poorly gauged basin. From the obtained results and from the analysis performed, the following conclusions can be raised:

- The proposed processing chain enables to build consistent prior hydraulic model geometry from multi-satellite data, including accurate images for dynamic water extents, and a hydrological model. It is applicable to other basins from the worlwide available data used in this study either for hydrological or hydraulic modeling.
- The VDA algorithm enables to simultaneously optimize high-dimensional spatio-temporal parameters of a river network 1D Saint-Venant hydraulic model, inflow hydrographs-bathymetry-friction, and significantly improve the fit to heterogeneous satellite WSE while providing hydrologically and hydraulicaly meaningfull estimates.
- The proposed approach represents a powerful optimization and diagnostic tool for hydrology-hydraulics from multi-source data. For example VDA can help detect data or modeling errors as done during our successive numerical experiments. Moreover, since the hydraulic model is differentiable, one can obtain spatially distributed sensitivity maps of cost function or simulated quantities w.r.t sought parameters and even build Sobol indices from them with derivative based approaches (Sobol' & Kucherenko (2009) applied in lumped hydrology in Chelil et al. (2022) or in 2D differentiable hydraulic modeling in Pujol et al. (2024)).

This work paves the way for further research and immediate to mid-term work perspectives are as follows.

- Assimilation of SWOT science orbit data, sparser in time and with nearly full spatial coverage at basin scale alone and in combination with the maximum of data to investigate finely their informative power and frequential inferrability issues.
- Application of the approach to gauged basins, using massive datasets including in situ and drone data in addition to satellite observations.
- Study of SWOT discharge approaches based on integrated basin scale hydrological-hydraulic network models.
- Advanced data-model error accounting in Bayesian framework.
- Fully differentiable hydrological-hydraulic models Pujol et al. (2022), with learnable parts Huynh et al. (2023), enabling simultaneous optimization of hydrological and hydraulic parameters from SWOT and other data, which pertains to tackling a double regionalization problem from data that are always sparser than model parameters and rarely fully informative/constraining. For example a lumped conceptual hydrological model already suffers from equifinality issues when calibrated from a discharge time series.

Note that DassFlow platform used in this work is open source (https://github.com/DassHydro/dassflow1d) and has recently been interfaced in Python enabling to use powerful libraries such as for signal processing and machine learning for building hybrid deterministic-ML methods in the powerful VDA framework.

A SWOT L2 wavelet based filtering and segmentation algorithm

The proposed algorithm aims to (i) efficiently denoise L2 SWOT-type river node-scale data (RiverObs product at spatial resolution $dx \sim 200m$), (ii) perform a segmentation of a river portion into reaches, at user defined scale, that best preserves hydraulic signals and ultimately contributes to the quality of flow modeling and its coherence with multi-mission altimetry data. In the present article only denoising of SWOT RiverObs WSE $Z(x)$ data is performed with pyrscwt before their assimilation into the hydraulic model at local XS scale.

The proposed algorithm taking as input a spatial signal of WSE $Z(x)$ signals, sampled at a constant spatial step, consists in the following steps:

- Signal resampling and symetrization (prolongation of the signal on its spatial borders).
- Automated choice of the wavelet projection basis (7 mother wavelets and 10 orders for each) such that the reconstruction error $\epsilon_{\hat{Z}}$ is minimal.
- Filtering and segmentation of the original signal $Z(x)$ obtained by a low-pass filtering of wavelet coefficients corresponding to spatial variations below a user defined cutoff length scale λ_c. An additional physical criterion is used to filter wavelet coefficients: at the scale of measurements a counter slope in the WS is unphysical, that is $\partial_x Z > 0$. For a zone of length l_d with a counter slope we consider a centered window of length $3l_d$, since we do not know whether this unphysical counterslope stems from over-understimations upstream or downstream, on which wavelet coefficients are iteratively filtered until $\partial_x \hat{Z} \leq 0$
- Hydraulic control sections (HCs) detection with the reconstructed signal $\hat{Z}(x)$ that is "error free" via maximum of WS curvature $\partial_x^2 \hat{Z}(x)$.

B Processing algorithm for ICESat-2 ATL13 data to extract WSE

ATL13 data is positionned along 6 beams (organized by pairs gt1r/gt1l, gt2r/gt2l, gt3r/gt3l) and presented as a set of beam-points (referenced by their longitude and latitude) above inland water bodies such as rivers and lakes only. Our purpose is to aggregate this data to build WSE timeseries at virtual station over the Maroni river. For this purpose, we need a set a line geometry representing the river network centerline and a polygon geometry delineating the a priori watermask where ATL13 data will be extracted and processed.

B1 Delineating the study domain watermask

The watermask is taken from the Pekel's global Surface Water Dataset, considering water pixels with an occurence of at least 50%, which is an adequate hypothesis given the relatively low variability of top width found on the Maroni (Sentinel 1-derived WSW of dynamic water masks, obtained with ExtractEO chain, were analysed and confirmed this).

For the studied Maroni basin, we considered and applied the following steps:

1. Polygonize Pekel watermask,
2. Application of a buffer with distance 0.0003 degree (as Pekel mask resolution is of 0.00025 degree): buffer function extends the boundaries of a given geometry and rounds its egde by the input distance.
3. Manual correction to fill missing river branches based on expert knowledge. Also, it was chosen to fully include under the watermask braided zone without distinguishing the individual river branches.
4. Cascaded union to merge individual polygons that intersect together
5. Small tributaries not represented by the Pekel product are added by building a polygon from a buffer around the riverline of those small tributaries and merging them to the rest of the domain (for the Maroni domain only).

B2 WSE data extraction

ICESat-2 products are organized by granule containing data below a full orbit, each orbit being divided in 6 beams (gt1l/gt1r/gt2l/gt2r/gt3l/gt3r). A individual ICESat-2 is a beam point caracterized by its coordinates (lon, lat) and an elevation wse (above the WGS84 ellipsoid). ICESat-2 have to be extracted and aggregated under virtual stations to derive elevation timeseries and XSs for the effective hydraulic model.

For each granule, the following processing is applied:

1. Extraction of all beam points within the study domain polygon
2. Each beam point is "projected" along the river centerline. From this linear referencing, a curvilinear abscissa x_s [m] (distance along the centerline from the upstream edge) and a distance-to-the-river d_r [m] (distance between the original beam point and its projection) are associated to each beam point.
3. Then, each beam point is associated to the closest virtual station according to their x_s. A distance d_s ($=x_{s,VS} - x_s$) and an angle ($=\arctan \frac{d_r}{d_s}$) are derived accordingly.
4. Once all beam points are extracted, potential outliers have to be detected and flagged out for further processing (see appendix B3)
5. For each virtual station, time-aggregation is easily done by gathering beam points that comes from the same granule and the same cycle.
6. subsequently, beam points gathered in the same time index are spatially-aggregated into a single elevation measurements (see appendix B3)

B3 More details on the processing of ATL13 data

B31 Outlier detection

Each river segment is divided into sub-segments of 5 km. Over each sub-segment, monthly subset of beam points which x_s fall on this sub-segment, are inspected. A linear regression of the elevation with respect to x_s from the ICESat-2 beam points subset is estimated with the standard deviation σ of the gap between the measured elevation and the corresponding (with respect to x_s) elevation from the linear regression. All points that are above 3σ are flagged out as outliers.

B32 Space aggregation

B322 Version 1

Every beam point attributes (ie. wse, lon, lat, x_s, d_s, d_r, angle, dt as seconds from Jan 1st, 2028) are simply averaged with a classical mean

B322 Version 2

Weighted averaged where each beam point weight w is defined by

$$w = 1. - \left\| \frac{d_s}{d_{s_max}} \right\|$$

B322 Draw XSs

For each segment and its associated subdomain polygon

1. the domain polygon is split into voronoi regions centered around the virtual stations of the polygon. Each region delineates any beam point which the closest virtual station is the region's associated virtual station.
2. The XSs is draw following the constraint below:
   - The section is contained within the associated voronoi region
   - The section contains the virtual station
   - The section should cross the river with an angle close to normal to the river centerline
   - The section have to cross any region boundaries that are common with the overall polygon exterior boundaries

   If one can not draw a XS that respects the constraints above, a section normal to the river centerline is drawn with a width equal to the largest d_r

C Processing of watermasks images to extract river width

River widths were extracted from a collection of 121 watermasks computed using the ExtractEO algorithm (Maxant et al. (2022)) on available Sentinel 1 images for the period 2021-01-01 - 2022-12-31. The river widths were computed using the dedicated BAS algorithm (https://github.com/CS-SI/BAS). The methodology is fully applicable on other zone of interest, even with watermask computed from other water classification algorithm (provided as binary classification where water is 1 and land,etc. is 0).

C1 Regularization for the Variational data assimilation algorithm

The ill-posed hydraulic inverse problem is regularized with the introduction of covariance operators and a change of control variable (Larnier et al. (2020) following Haben et al. (2011b)) as:

$$k = B^{-1/2}\left(\boldsymbol{\theta} - \boldsymbol{\theta}^{(0)}\right) \tag{C1}$$

The background $\boldsymbol{\theta}^{(0)}$ (first guess, or prior in statistics) on the sought parameter (from which optimization is started), and the background error covariance matrix B, both depend on the information available and a priori physical knowledge of the system and of the unknowns. With this change of control variable we are interested in the minimization ot the following cost function:

$$j\left(\boldsymbol{k}\right) = \frac{1}{2}\left\|\mathcal{M}(\boldsymbol{\theta}^{(0)} + B^{1/2}\boldsymbol{k}) - Y^*\right\|_O^2 \tag{C2}$$

The choice of B, that can be seen as a preconditionning (cf. Haben et al. (2011a,b)), is crucial for the optimization and influences the inferred solution.

Assuming uncorrelated unknowns, the matrix B is block diagonal:

$$B = \begin{pmatrix} B_Q & 0 & 0 \\ 0 & B_b & 0 \\ 0 & 0 & B_K \end{pmatrix} \tag{C3}$$

each block $B_\square$ is defined with decreasing exponential kernels and physical scales (cf. Larnier et al. (2020),Malou & Monnier (2022) and cited references):

$$\left(B_Q\right)_{i,j} = \left(\sigma_Q\right)^2 exp\left(-\frac{|t_j - t_i|}{L_Q}\right);\ and\ \ \left(B_b\right)_{i,j} = \left(\sigma_b\right)^2 exp\left(-\frac{|x_j - x_i|}{L_b}\right);\ and\ \ B_K = diag\left(\sigma_\alpha^2, \sigma_\beta^2\right) \tag{C4}$$

with L_Q and L_b acting as correlation scales defined a priori from empirical physical knowledge. The scalar values $\sigma_\square$ can be seen as variances and have a weighting effect in parameters optimization.

D Detail on inferred parameters

Open Research

Data Availability Statement. This article is based on open source data, dataset shareable uppon request. *Software Availability Statement.* Our DassFlow1D source code is open source and available at https://github.com/DassHydro/dassflow MGB is also an open source code.

Acknowledgments

CNES for financial support of several authors, and also for engineering support regarding processing of WSW data and SWOT data. DEAL Guyane for processing discharge data. Evanne Angenent for data processing and contribution to the first modeling of the Maroni basin with MGB-DassFlow1D, during an internship at INRAE and DEAL Cayenne. Joao Hemptinne for participation to re-implementation of the segmentation algorihtm.

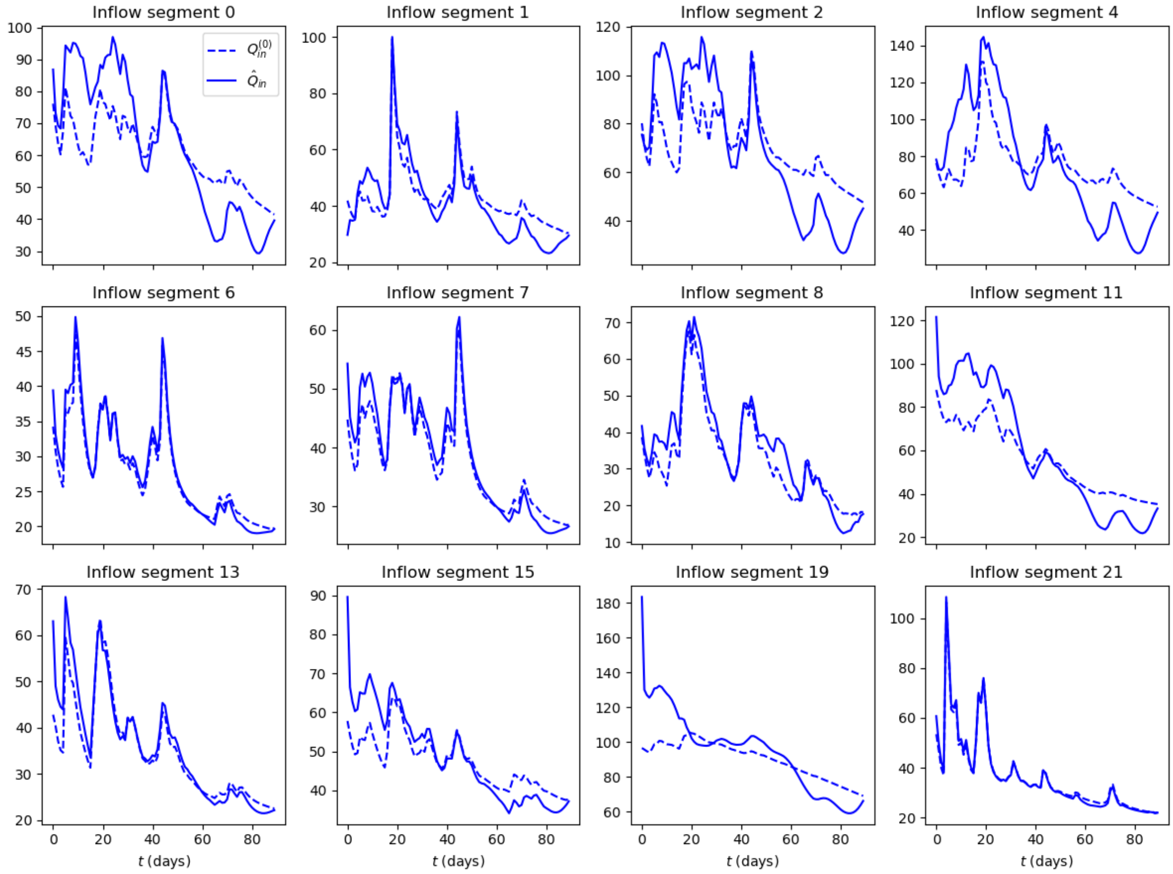

Figure D1. Inferred inflow hydrographs NadAlti.4limni

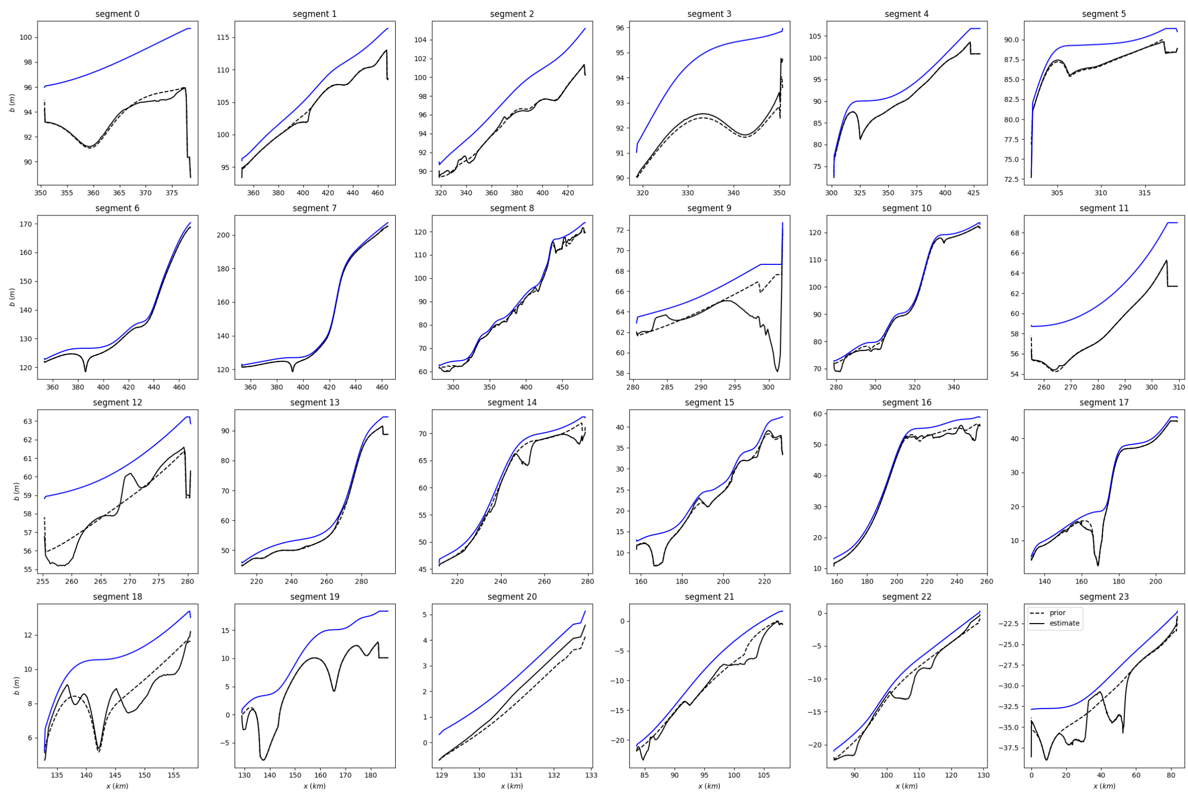

Figure D2. Inferred bathymetry NadAlti.4limni

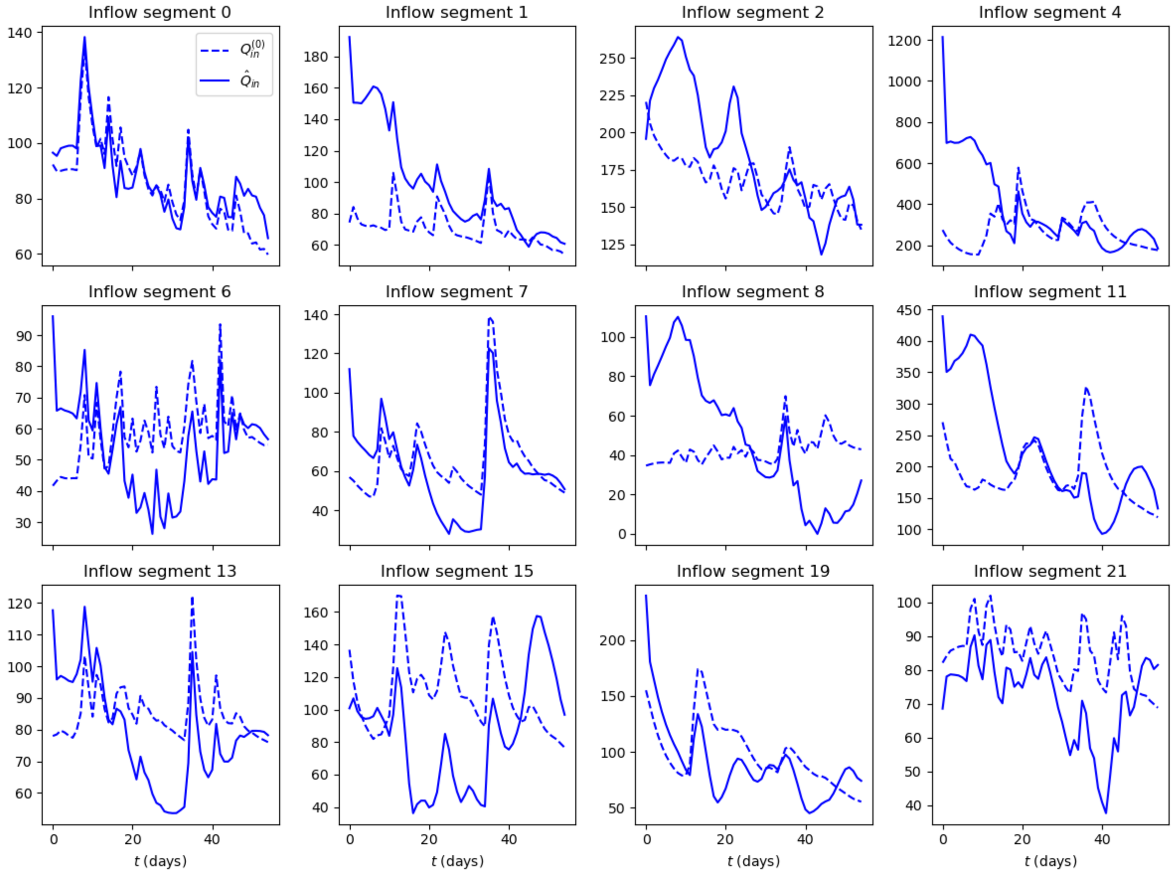

Figure D3. Inferred inflow hydrographs SWOT only

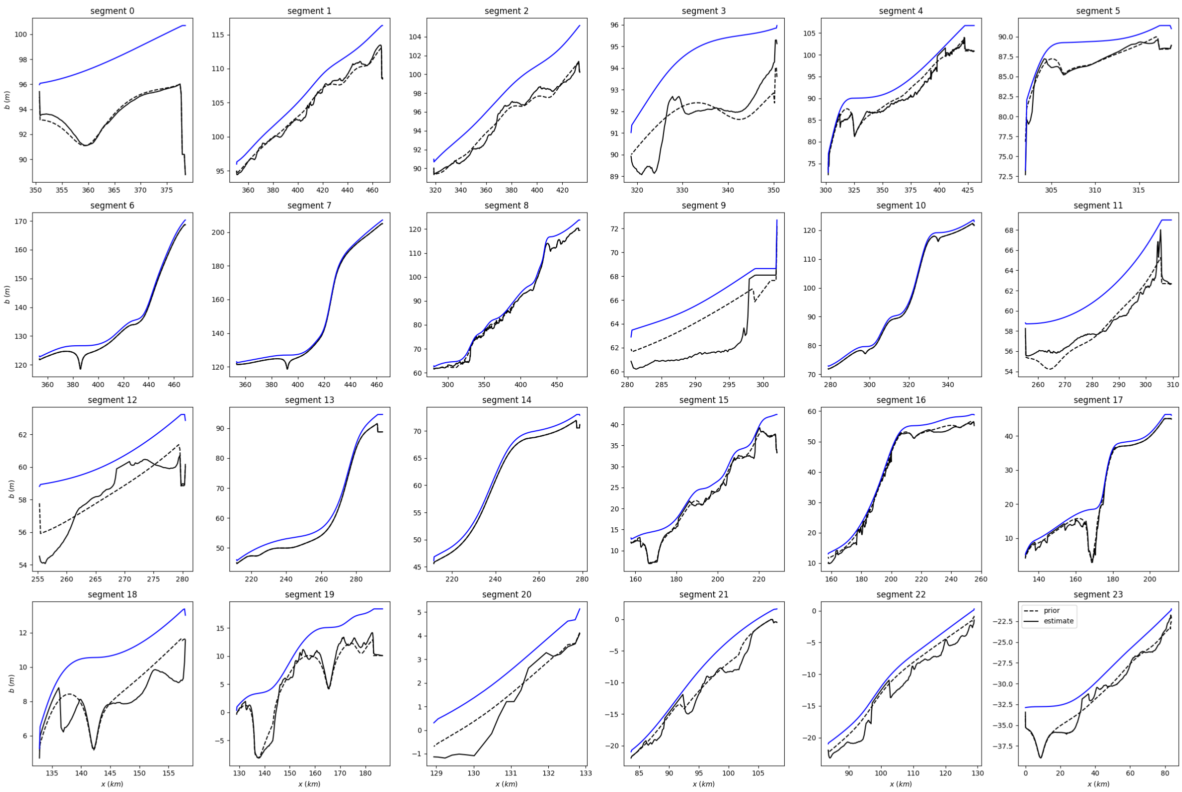

Figure D4. Inferred bathymetry SWOT only

Authors contributions: Design of this research, conceptualization, analysis and initial manuscript writing: PAG and KL. Numerical results: KL. Preprocessing algorithms implementation: CE, KL. Data and/or hydrological modeling and/or review and editing of the manuscript: All.

References

Andreadis, K. M., Brinkerhoff, C. B., & Gleason, C. J. (2020). Constraining the assimilation of swot observations with hydraulic geometry relations. *Water Resources Research*, *56*(5), e2019WR026611. Retrieved from https://agupubs.onlinelibrary.wiley.com/doi/abs/10.1029/2019WR026611 (e2019WR026611 10.1029/2019WR026611) doi: https://doi.org/10.1029/2019WR026611

Brisset, P., Monnier, J., Garambois, P.-A., & Roux, H. (2018). On the assimilation of altimetric data in 1D Saint-Venant river flow models. *Advances in water resources*, *119*, 41-59. Retrieved from https://doi.org/10.1016/j.advwatres.2018.06.004

Cacuci, D., Navon, I., & Ionescu-Bugor, M. (2013). *Computational methods for data evaluation and assimilation.* Taylor and Francis CRC Press: Boca Raton.

Chelil, S., Oubanas, H., Henine, H., Gejadze, I., Malaterre, P. O., & Tournebize, J. (2022). Variational data assimilation to improve subsurface drainage model parameters. *Journal of Hydrology*, 128006.

Chow, V. (1959). *Open-channel hydraulics.* New-York, USA: Mc Graw-Hill.

Collischon, W., Allasia, D., Da Silva, B., & M., T. C. E. (2007). The mgb-iph model for large-scale rainfall—runoff modelling. *Hydrological Sciences Journal*, *52*(5), 878–895. Retrieved from https://doi.org/10.1623/hysj.52.5.878 doi: 10.1623/hysj.52.5.878

Coppo Frias, M., Liu, S., Mo, X., Nielsen, K., Randall, H., Jiang, L., … Bauer-Gottwein, P. (2022). River hydraulic modelling with icesat-2 land and water surface elevation. *EGUsphere*, *2022*, 1–27. Retrieved from https://egusphere.copernicus.org/preprints/2022/egusphere-2022-377/ doi: 10.5194/egusphere-2022-377

Cunge, J. A., Holly, M., F., & Verwey, A. (1980). *Practical aspects of computational river hydraulics.* Pitam Publishing,.

Dingman, S. (2009). *Fluvial hydraulics.* Oxford University Press.

Dingman, S. L. (2007). Analytical derivation of at-a-station hydraulic–geometry relations. *Journal of Hydrology*, *334*(1), 17-27. Retrieved from https://www.sciencedirect.com/science/article/pii/S0022169406005063 doi: https://doi.org/10.1016/j.jhydrol.2006.09.021

Dingman, S. L., & Afshari, S. (2018). Field verification of analytical at-a-station hydraulic-geometry relations. *Journal of Hydrology*, *564*, 859-872. Retrieved from https://www.sciencedirect.com/science/article/pii/S0022169418305250 doi: https://doi.org/10.1016/j.jhydrol.2018.07.020

Durand, M., Gleason, C. J., Pavelsky, T. M., Prata de Moraes Frasson, R., Turmon, M., David, C. H., … Wang, J. (2023). A framework for estimating global river discharge from the surface water and ocean topography satellite mission. *Water Resources Research*, *59*(4), e2021WR031614. Retrieved from https://agupubs.onlinelibrary.wiley.com/doi/abs/10.1029/2021WR031614 (e2021WR031614 2021WR031614) doi:

https://doi.org/10.1029/2021WR031614

Durand, M., Neal, J., Rodríguez, E., Andreadis, K., Smith, L., & Yoon, Y. (2014). Estimating reach-averaged discharge for the river Severn from measurements of river water surface elevation and slope. *Journal of Hydrology*, *511*, 92-104. doi: 10.1016/j.jhydrol.2013.12.050

Eggleston, J., Mason, C., Bjerklie, D., Durand, M., Dudley, R., & Harlan, M. (2024). Siting considerations for satellite observation of river discharge. *Water Resources Research*, *60*(6), e2023WR034583. Retrieved from https://agupubs.onlinelibrary.wiley.com/doi/abs/10.1029/2023WR034583 (e2023WR034583 2023WR034583) doi: https://doi.org/10.1029/2023WR034583

Flipo, N., Mouhri, A., Labarthe, B., Biancamaria, S., Rivière, A., & Weill, P. (2014). Continental hydrosystem modelling: the concept of nested stream–aquifer interfaces. *Hydrology and Earth System Sciences*, *18*(8), 3121–3149. Retrieved from https://www.hydrol-earth-syst-sci.net/18/3121/2014/ doi: 10.5194/hess-18-3121-2014

Frasson, R. P. d. M., Durand, M. T., Larnier, K., Gleason, C., Andreadis, K. M., Hagemann, M., ... David, C. H. (2021). Exploring the factors controlling the error characteristics of the surface water and ocean topography mission discharge estimates. *Water Resources Research*, *57*(6), e2020WR028519. Retrieved from https://agupubs.onlinelibrary.wiley.com/doi/abs/10.1029/2020WR028519 (e2020WR028519 2020WR028519) doi: https://doi.org/10.1029/2020WR028519

Garambois, P.-A., Calmant, S., Roux, H., Paris, A., Monnier, J., Finaud-Guyot, P., ... Santos-da Silva, J. (2017). Hydraulic visibility: Using satellite altimetry to parameterize a hydraulic model of an ungauged reach of a braided river. *Hydrological Processes*, *31*(4), 756–767. Retrieved from http://dx.doi.org/10.1002/hyp.11033 (hyp.11033) doi: 10.1002/hyp.11033

Garambois, P.-A., Larnier, K., Monnier, J., Finaud-Guyot, P., Verley, J., Montazem, A.-S., & Calmant, S. (2020). Variational estimation of effective channel and ungauged anabranching river discharge from multi-satellite water heights of different spatial sparsity. *Journal of Hydrology*, *581*, 124409. Retrieved from https://www.sciencedirect.com/science/article/pii/S0022169419311448 doi: https://doi.org/10.1016/j.jhydrol.2019.124409

Garambois, P.-A., & Monnier, J. (2015). Inference of effective river properties from remotely sensed observations of water surface. *Advances in Water Resources*, *79*, 103-120. Retrieved from https://www.sciencedirect.com/science/article/pii/S0309170815000330 doi: https://doi.org/10.1016/j.advwatres.2015.02.007

Getirana, A. C. (2010). Integrating spatial altimetry data into the automatic calibration of hydrological models. *Journal of Hydrology*, *387*(3), 244-255. Retrieved from https://www.sciencedirect.com/science/article/pii/S0022169410001988 doi: https://doi.org/10.1016/j.jhydrol.2010.04.013

Haben, S., Lawless, A., & Nichols, N. (2011a). Conditioning and preconditioning of the variational data assimilation problem. *Computers & Fluids*, *46*(1), 252-256.

Haben, S., Lawless, A., & Nichols, N. (2011b). Conditioning of incremental variational data assimilation, with application to the met office system. *Tellus A*, *63*(4), 782-792.

Hascoet, L., & Pascual, V. (2013). The tapenade automatic differentiation tool: principles, model, and specification. *ACM Transactions on Mathematical Software (TOMS)*, *39*(3), 1–43.

Horner, I., Renard, B., Le Coz, J., Branger, F., McMillan, H. K., & Pierrefeu, G. (2018). Impact of Stage Measurement Errors on Streamflow Uncertainty. *Water Resour. Res.*, *54*(3), 1952–1976. doi: 10.1002/2017WR022039

Huynh, N. N. T., Garambois, P.-A., Colleoni, F., Renard, B., Roux, H., Demargne, J., & Javelle, P. (2023). *Learning regionalization within a differentiable high-resolution hydrological model using accurate spatial cost gradients.*

Huynh, N. N. T., Garambois, P.-A., Renard, B., Colleoni, F., Monnier, J., & Roux, H. (2024, February). Multiscale learnable physical modeling and data assimilation framework: Application to high-resolution regionalized hydrological simulation of flash floods. Retrieved from http://dx.doi.org/10.22541/au.170709054.44271526/v1 doi: 10.22541/au.170709054.44271526/v1

Kirstetter, G., Hu, J., Delestre, O., Darboux, F., Lagrée, P.-Y., Popinet, S., ... Josserand, C. (2016). Modeling rain-driven overland flow: Empirical versus analytical friction terms in the shallow water approximation. *Journal of Hydrology*, *536*, 1–9.

Kubota, T., Aonashi, K., Ushio, T., Shige, S., Takayabu, Y. N., Kachi, M., ... others (2020). Global satellite mapping of precipitation (gsmap) products in the gpm era. *Satellite Precipitation Measurement: Volume 1*, 355–373.

Lague, D., & Feldmann, B. (2020). Chapter 2 - topo-bathymetric airborne lidar for fluvial-geomorphology analysis. In P. Tarolli & S. M. Mudd (Eds.), *Remote sensing of geomorphology* (Vol. 23, p. 25-54). Elsevier. Retrieved from https://www.sciencedirect.com/science/article/pii/B9780444641779000023 doi: https://doi.org/10.1016/B978-0-444-64177-9.00002-3

Larnier, K., & Monnier. (2023). Hybrid neural network - variational data assimilation algorithm to infer river discharges from swot-like data. *Comput Geoscience*, 853–877. Retrieved from https://doi.org/10.1007/s10596-023-10225-2

Larnier, K., Monnier, J., Garambois, P.-A., & Verley, J. (2020). River discharge and bathymetry estimation from swot altimetry measurements. *Inverse Problems in Science and Engineering*, 1-31. Retrieved from https://doi.org/10.1080/17415977.2020.1803858

Le Coz, J., Renard, B., Bonnifait, L., Branger, F., & Le Boursicaud, R. (2014). Combining hydraulic knowledge and uncertain gaugings in the estimation of hydrometric rating curves: A bayesian approach. *Journal of Hydrology*, *509*, 573-587. Retrieved from https://www.sciencedirect.com/science/article/pii/S0022169413008329 doi: https://doi.org/10.1016/j.jhydrol.2013.11.016

Leopold, L., & Maddock, T. (1953). The hydraulic geometry of stream channels and some physiographic implications. *USGS Numbered Series*, *252*, 57pp. Retrieved from https://pubs.er.usgs.gov/publication/pp252

Malou, T., Garambois, P.-A., Paris, A., Monnier, J., & Larnier, K. (2021). Generation and analysis of stage-fall-discharge laws from coupled hydrological-hydraulic river network model integrating sparse multi-satellite data. *Journal of Hydrology*, *603*, 126993. Retrieved from https://doi.org/10.1016/j.jhydrol.2021.126993

Malou, T., & Monnier, J. (2022). Covariance kernels investigation from diffusive wave equations for data assimilation in hydrology. *Inverse Problems*. Retrieved from https://doi.org/10.1088/1361-6420/ac509d (Accepted)

Mansanarez, V., Le Coz, J., Renard, B., Lang, M., Pierrefeu, G., & Vauchel, P. (2016). Bayesian analysis of stage-fall-discharge rating curves and their uncertainties. *Water Resources Research*, *52*(9), 7424-7443. Retrieved from https://agupubs.onlinelibrary.wiley.com/doi/abs/10.1002/2016WR018916 doi: https://doi.org/10.1002/2016WR018916

Masson-Delmotte, V., Zhai, P., Pörtner, H.-O., Roberts, D., Skea, J., Shukla, P. R., et al. (2022). *Global warming of 1.5 c: Ipcc special report on impacts of global warming of 1.5 c above pre-industrial levels in context of strengthening response to climate change, sustainable development, and efforts to eradicate poverty.* Cambridge University Press.

Maxant, J., Braun, R., Caspard, M., & Clandillon, S. (2022). Extracteo, a pipeline for disaster extent mapping in the context of emergency management. *Remote Sensing*, *14*(20). Retrieved from https://www.mdpi.com/2072-4292/14/20/5253 doi: 10.3390/rs14205253

Meyer Oliveira, A., Fleischmann, A., & Paiva, R. (2021). On the contribution of remote sensing-based calibration to model hydrological and hydraulic processes in tropical regions. *Journal of Hydrology*, *597*, 126184. Retrieved from https://www.sciencedirect.com/science/article/pii/S0022169421002316 doi: https://doi.org/10.1016/j.jhydrol.2021.126184

Milly, P. (1994). Climate, interseasonal storage of soil water, and the annual water balance. *Advances in Water Resources*, *17*(1), 19-24. Retrieved from https://www.sciencedirect.com/science/article/pii/0309170894900205 (MIT Colloquium on Hydroclimatology and Global Hydrology) doi: 10.1016/0309-1708(94)90020-5

Monnier, J. (2021). *Variational data assimilation and model learning.*

Montazem, A.-S., Garambois, P.-A., Calmant, S., Finaud-Guyot, P., Monnier, J., Medeiros Moreira, D., ... Biancamaria, S. (2019). Wavelet-based river segmentation using hydraulic control-preserving water surface elevation profile properties. *Geophysical Research Letters*, *46*(12), 6534-6543. Retrieved from https://agupubs.onlinelibrary.wiley.com/doi/abs/10.1029/2019GL082986 doi: 10.1029/2019GL082986

Nachtergaele, F., van Velthuizen, H., Verelst, L., Wiberg, D., Henry, M., Chiozza, F., ... others (2023). *Harmonized world soil database version 2.0.* FAO.

Nicollet, G., & Uan, M. (1979). Ecoulements permanents surface libre en lits composés. *La Houille Blanche*.

Oubanas, H., Gejadze, I., Malaterre, P.-O., & Mercier, F. (2018). River discharge estimation from synthetic swot-type observations using var- iational data assimilation and the full saint-venant hydraulic model. *Journal of Hydrology*, Accepted, to appear.

Paiva, R. C. D., Collischonn, W., Bonnet, M.-P., de Gonçalves, L. G. G., Calmant, S., Getirana, A., & Santos da Silva, J. (2013). Assimilating in situ and radar altimetry data into a large-scale hydrologic-hydrodynamic model for streamflow forecast in the amazon. *Hydrology and Earth System Sciences*, *17*(7), 2929–2946. Retrieved from https://hess.copernicus.org/articles/17/2929/2013/ doi: 10.5194/hess-17-2929-2013

Paris, A., Dias de Paiva, R., Santos da Silva, J., Medeiros Moreira, D., Calmant, S., Garambois, P.-A., ... Seyler,

F. (2016). Stage-discharge rating curves based on satellite altimetry and modeled discharge in the amazon basin. *Water Resources Research*, *52*(5), 3787-3814. Retrieved from https://agupubs.onlinelibrary.wiley.com/doi/abs/10.1002/2014WR016618 doi: https://doi.org/10.1002/2014WR016618

Pavelsky, T. M. (2014). Using width-based rating curves from spatially discontinuous satellite imagery to monitor river discharge. *Hydrological Processes*, *28*(6), 3035-3040. Retrieved from https://onlinelibrary.wiley.com/doi/abs/10.1002/hyp.10157 doi: https://doi.org/10.1002/hyp.10157

Pontes, P. R. M., Fan, F. M., Fleischmann, A. S., de Paiva, R. C. D., Buarque, D. C., Siqueira, V. A., … Collischonn, W. (2017). Mgb-iph model for hydrological and hydraulic simulation of large floodplain river systems coupled with open source gis. *Environmental Modelling & Software*, *94*, 1-20. Retrieved from https://www.sciencedirect.com/science/article/pii/S136481521630189X doi: https://doi.org/10.1016/j.envsoft.2017.03.029

Pujol, L., Garambois, P.-A., Delenne, C., & Perrin, J.-L. (2024). Adjoint-based sensitivity analysis and assimilation of multi-source1 data for the inference of spatio-temporal parameters in a 2d urban2 flood hydraulic model. *In revision*.

Pujol, L., Garambois, P.-A., Delenne, C., & Perrin, J.-L. (2024). Adjoint-based sensitivity analysis and assimilation of multi-source data for the inference of spatio-temporal parameters in a 2d urban flood hydraulic model. *submitted*.

Pujol, L., Garambois, P.-A., Finaud-Guyot, P., Monnier, J., Larnier, K., Mosé, R., … Calmant, S. (2020). Estimation of multiple inflows and effective channel by assimilation of multi-satellite hydraulic signatures: The ungauged anabranching negro river. *Journal of Hydrology*, *591*, 125331. Retrieved from https://doi.org/10.1016/j.jhydrol.2020.125331

Pujol, L., Garambois, P.-A., & Monnier, J. (2022). Multi-dimensional hydrological-hydraulic model with variational data assimilation for river networks and floodplains. *EGUsphere*, *2022*, 1–44. Retrieved from https://egusphere.copernicus.org/preprints/egusphere-2022-10/ doi: 10.5194/egusphere-2022-10

Rodríguez, E., Durand, M., & Frasson, R. P. d. M. (2020). Observing rivers with varying spatial scales. *Water resources research*, *56*(9). Retrieved from https://doi.org/10.1029/2019WR026476

Roux, H. (2004). *Estimation de paramètres en hydraulique fluviale, à partir de données caractéristiques de l'imagerie aérienne* (Unpublished doctoral dissertation).

Samuels, P. G. (1989). Backwater lengths in rivers. *Proceedings of the Institution of Civil Engineers*, *87*(4), 571-582. Retrieved from https://doi.org/10.1680/iicep.1989.3779 doi: 10.1680/iicep.1989.3779

Schneider, R., Godiksen, P. N., Villadsen, H., Madsen, H., & Bauer-Gottwein, P. (2017). Application of cryosat-2 altimetry data for river analysis and modelling. *Hydrology and Earth System Sciences*, *21*(2), 751–764. Retrieved from https://hess.copernicus.org/articles/21/751/2017/ doi: 10.5194/hess-21-751-2017

Schuite, J., Flipo, N., Massei, N., Rivière, A., & Baratelli, F. (2019). Improving the spectral analysis of hydrological signals to efficiently constrain watershed properties. *Water Resources Research*, *55*(5), 4043-4065. Retrieved from https://agupubs.onlinelibrary.wiley.com/doi/abs/10.1029/2018WR024579 doi:

10.1029/2018WR024579

Sobol', I., & Kucherenko, S. (2009). Derivative based global sensitivity measures and their link with global sensitivity indices. *Mathematics and Computers in Simulation*, *79*(10), 3009-3017. doi: 10.1016/j.matcom.2009.01.023

Tuozzolo, S., Lind, G., Overstreet, B., Mangano, J., Fonstad, M., Hagemann, M., ... Durand, M. (2019). Estimating river discharge with swath altimetry: A proof of concept using airswot observations. *Geophysical Research Letters*, *0*(ja). Retrieved from https://agupubs.onlinelibrary.wiley.com/doi/abs/10.1029/2018GL080771 doi: 10.1029/2018GL080771

Wongchuig-Correa, S., Cauduro Dias de Paiva, R., Biancamaria, S., & Collischonn, W. (2020). Assimilation of future swot-based river elevations, surface extent observations and discharge estimations into uncertain global hydrological models. *Journal of Hydrology*, *590*, 125473. Retrieved from https://www.sciencedirect.com/science/article/pii/S0022169420309331 doi: https://doi.org/10.1016/j.jhydrol.2020.125473

Yamazaki, D., Ikeshima, D., Sosa, J., Bates, P. D., Allen, G. H., & Pavelsky, T. M. (2019). Merit hydro: A high-resolution global hydrography map based on latest topography dataset. *Water Resources Research*, *55*(6), 5053-5073. Retrieved from https://agupubs.onlinelibrary.wiley.com/doi/abs/10.1029/2019WR024873 doi: https://doi.org/10.1029/2019WR024873

Yoon, Y., Garambois, P.-A., Paiva, R. C., Durand, M., Roux, H., & Beighley, E. (2016). Improved error estimates of a discharge algorithm for remotely sensed river measurements: Test cases on sacramento and garonne rivers. *Water Resources Research*, *52*(1), 278-294. Retrieved from https://agupubs.onlinelibrary.wiley.com/doi/abs/10.1002/2015WR017319 doi: https://doi.org/10.1002/2015WR017319

Zanaga, D., Van De Kerchove, R., De Keersmaecker, W., Souverijns, N., Brockmann, C., Quast, R., ... Arino, O. (2021, October). *Esa worldcover 10 m 2020 v100.* Zenodo. Retrieved from https://doi.org/10.5281/zenodo.5571936 doi: 10.5281/zenodo.5571936